

# **REUSABLE BIPOLAR VESSEL SEALING DEVICE WITH A UNIFORM PRESSURE PROFILE**

DESIGN, DEVELOPMENT AND VALIDATION



MASTER THESIS | BIOMEDICAL ENGINEERING

**JAMES CROSS**



# Reusable Bipolar Vessel Sealing Device with a Uniform Pressure Profile

## Design, Development and Validation

by

**James Andrew Cross**

to obtain the degree of Master of Science  
at the Delft University of Technology,  
to be defended publicly on Tuesday August 23, 2022 at 13:00 PM.



Student number: 4432258  
Project duration: January 2021 – August 2022  
Thesis committee: Prof. dr. ir. T. Horeman, TU Delft  
P.D. Robertson, TU Delft, supervisor  
Prof. dr. J. Dankelman, TU Delft

An electronic version of this thesis is available at <http://repository.tudelft.nl/>.

## Abstract

Bipolar electrosurgical vessel sealing is commonly used in human and veterinary medicine. This method of vessel sealing is often preferred over traditional suturing or clipping of blood vessels because it comes with the advantages of reducing intraoperative blood loss and operation time. Most bipolar vessel sealers are disposable. The high costs of the devices often lead to unrightful reuse in LMICs, increasing the risk of postoperative infection. Next to that, many existing vessel sealing devices operate using a scissor-like clamp that exerts a larger clamping pressure at the proximal end than at the distal end of the clamp. Studies have shown that an unevenly distributed clamping pressure negatively affects the burst pressure of the seal [1][2][3]. The aim of this thesis is to redesign the conventional bipolar vessel sealer to a reusable version that exerts a uniformly distributed pressure across the clamping surface.

A design goal and a set of design requirements were constructed to clarify the objectives. This was followed by a creative design process which was executed to generate solutions for the problems of disposability and uneven pressure distribution. The concept for reusability was verified by mechanical analysis of forces and by rapid prototyping. For the pressure distribution, three concepts were made and tested for performance during an experiment. A redesign of the conventional bipolar vessel sealer was made in CAD containing the innovations for reusability and the pressure distribution mechanism that performed best.

A mechanism has been designed that allows the closing of the upper jaw to be actuated by forward motion of the blade. This eliminates the need for a separate jaw actuator hence promotes cleanability and reusability. The pressure distribution experiment demonstrated which mechanism performed the best. These innovations together with other design considerations have been incorporated into a CAD model of the redesigned bipolar vessel sealer.

The design goal has been met successfully. All design requirements have been met except for one. The removability of the blade lacks in the redesign because it was hindered by other innovations. A list of recommendations has been made to highlight potential future opportunities and shortcomings.

# Contents

<b>1</b>	<b>Introduction</b>	<b>7</b>
1.1	Laparoscopic devices in developing countries . . . . .	7
1.2	Bipolar vessel sealing . . . . .	8
1.3	Reusability of surgical equipment . . . . .	8
1.4	Uniformly distributed clamping . . . . .	9
1.5	Problem definition . . . . .	9
1.5.1	Reusable bipolar vessel sealer . . . . .	9
1.5.2	Uniform compression . . . . .	10
1.5.3	Area of innovation . . . . .	10
1.6	Design goal . . . . .	10
1.7	Design requirements . . . . .	10
1.8	Design methodology . . . . .	11
1.9	Function analyses . . . . .	13
<b>2</b>	<b>Concept design: reusability</b>	<b>14</b>
2.1	Choice of area of innovation . . . . .	14
2.1.1	Market research hinge . . . . .	14
2.2	Choice of innovation . . . . .	15
<b>3</b>	<b>Concept design: pressure distribution</b>	<b>16</b>
3.1	Choice of type of mechanism . . . . .	16
3.1.1	Literature studies . . . . .	16
3.1.2	Market research pressure distribution . . . . .	17
3.1.3	Choice of principle . . . . .	17
3.2	Choice of mechanisms . . . . .	18
3.2.1	Research tissue thickness . . . . .	18
3.2.2	Assumptions on force, material, dimensions and distortions . . . . .	18
3.2.3	Choice of mechanisms . . . . .	19
3.3	Model for verification of dimensions . . . . .	19
<b>4</b>	<b>Concept validation</b>	<b>21</b>
4.1	Methods . . . . .	21
4.1.1	Experimental variables . . . . .	22
4.2	Processing of data . . . . .	23
4.3	Validity of load cells for force measurement . . . . .	24
4.4	Results . . . . .	25
4.4.1	Results angle experiment . . . . .	25
4.5	Discussion . . . . .	26
4.5.1	Explanation of results . . . . .	26
4.5.2	Leaf spring performance . . . . .	28
4.5.3	Leaf spring performance at an angle . . . . .	30
4.5.4	Conclusion . . . . .	31
4.5.5	Further considerations . . . . .	31
<b>5</b>	<b>Embodiment design</b>	<b>34</b>
5.1	Design choices . . . . .	34
5.1.1	Distribution mechanism . . . . .	34
5.1.2	Hinge . . . . .	35
5.1.3	Connection shaft/hinge . . . . .	36
5.1.4	Partition of current flow . . . . .	36
5.1.5	Blade . . . . .	37
5.1.6	Jaws . . . . .	37
5.1.7	Coating for friction . . . . .	38

5.1.8	Choice of material . . . . .	38
5.2	Technical design . . . . .	38
5.2.1	Free Body Diagram verification . . . . .	39
5.2.2	Rapid prototyping . . . . .	39
<b>6</b>	<b>Discussion</b>	<b>40</b>
6.1	Design goal . . . . .	40
6.2	Design requirements . . . . .	41
6.3	Recommendations . . . . .	42
6.3.1	Circuitry . . . . .	42
6.3.2	Low thickness . . . . .	42
6.3.3	High pushing force . . . . .	43
6.3.4	Scalability . . . . .	43
6.3.5	Cleanable distribution mechanism . . . . .	43
6.3.6	Cleaning tool . . . . .	43
6.3.7	Blade removal . . . . .	43
6.3.8	Haptic feedback . . . . .	43
6.3.9	Insert fixation . . . . .	44
6.4	Conclusion . . . . .	44
	<b>References</b>	<b>44</b>
	<b>A Appendix</b>	<b>48</b>
	<b>B Pressure distribution experiment - lab report</b>	<b>60</b>
B.1	Introduction . . . . .	60
B.2	Materials . . . . .	60
B.3	Method . . . . .	60
B.4	Control treatment . . . . .	61
B.5	Calibration of load cells . . . . .	61
	<b>C Results tables</b>	<b>62</b>

# 1 Introduction

## 1.1 Laparoscopic devices in developing countries

Laparoscopy, also known as keyhole surgery, is a form of minimally invasive surgery (MIS). Instead of open surgery, which requires the surgeon to make large incisions in the skin, the abdomen is accessed through small holes that are created in the abdomen wall. A laparoscope (a rod with a light source and a camera) is used to perform the intervention together with the laparoscopic versions of the other tools necessary. For a device to be used in laparoscopic interventions, the shaft and tip should together range between 34 and 37 cm in length and should have an maximum outer diameter of 5 mm. Devices with a diameter of 3 and 10 mm exist but 5 mm is used most commonly. Figure 1 shows an illustration of a laparoscopic setup. Trocars are inserted into the incisions and serve as a portal for the instruments inside the abdomen. To make the insides visible and manipulatable, the abdomen is inflated using carbon dioxide. This is called a pneumoperitoneum [4].

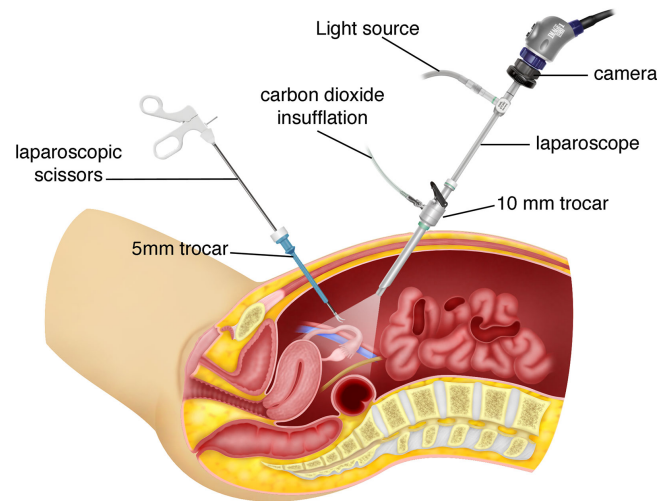


Figure 1: An illustration of the instruments used during a laparoscopic intervention. Trocars are inserted into the keyholes as portals to allow easy access of instruments into the abdomen. Creation of pneumoperitoneum (an inflated abdomen) gives the surgeon space to see and manipulate tissues [5].

This form of MIS is often preferred in certain procedures due to the minimised trauma to the abdominal wall. Not having to cut open the patient comes with the advantages of faster recovery time and reduced hospital stay. In most cases, laparoscopy increases efficiency and the probability of a positive surgical outcome. It also reduces the rate of wound infections and perioperative morbidity together with blood loss and postoperative pain [6].

While High-Income countries (HIC's) have been using laparoscopy for interventions that allow it, most Low-to-Middle-Income countries (LMICs) are still performing open surgeries in their hospitals. These facilities are often characterised by poor sanitary living conditions, limited access to clean drinking water and scarcity of blood banks. Consequentially, the postoperative infection rates in these countries can be up to 25 times higher than in HICs [7].

The measure to solve this problem would be to introduce laparoscopy to LMICs. There is one big hurdle that hinders the innovation towards laparoscopy and that is the cost thereof.

Laparoscopic devices are generally more expensive than regular surgical equipment. Next to that, the sterilisation procedures of this equipment are more complicated due to their long and thin geometry with internal cavities for actuation. The successful use of laparoscopic devices requires proper training, resulting in the third problem; staff training requires time and money and is difficult to organise due to a shortage of individuals to serve as trainers [8].

Due to the complexity of the sterilisation of laparoscopic equipment and to ensure the safety of the patient in terms of infection, most laparoscopic devices are designed to be disposable [9]. While HIC's can afford to dispose the instruments after single use, it is too much of a financial burden for LMIC hospitals. This often leads to unrightful reuse of disposable devices which are not designed for cleanability, jeopardising patients' safety by increasing the risk of infection [10].

## 1.2 Bipolar vessel sealing

A common laparoscopic instrument that is being reused unrightfully is the bipolar vessel sealer (BVS). This device clamps blood vessels up to 7 mm in diameter or other tissues with a mechanical force. It then heats up the tissue using an electric current, causing the proteins collagen and elastin to denature. The mechanical pressure forms a coagulum and in many devices a blade divides the tissue, leaving the surgeon with two perfectly sealed ends [11].

Bipolar vessel sealing is especially advantageous when used in a laparoscopic setup. Traditional minimally invasive surgery includes suture ligation with 34 centimeter long forceps. This requires skill and tends to be time-consuming. The bipolar vessel sealer comes with the advantages of reduced intraoperative blood loss, shorter surgery duration and less postoperative complications [11].



Figure 2: A conventional bipolar vessel sealer by LigaSure.

The proper use of a bipolar vessel sealer speeds up surgery and decreases blood loss, something worthy in areas without blood banks. These advantages combined form the incentive to redesign the bipolar vessel sealer to be pronounced reusable. Reusability in surgical equipment translates to cleanability and durability. The product will have to allow to be properly cleaned and sterilised to minimise risk of nosocomial infection. Looking from a durability perspective, the product must be constructed from materials that can withstand enough use and sterilisation cycles to be called reusable.

## 1.3 Reusability of surgical equipment

Making surgical instruments reusable has many advantages. Apart from prevention of unrightful reuse hence increased risk of infections for patients, it also adds to a more circular and sustainable society. In the past 30 years, hospitals have seen a trend shift from reusable products to their disposable forms [12]. This movement was fueled by a rising interest in decreasing risk of infection and easier design and production. As a result, hospitals are now largely reliant on single use products, drastically increasing their carbon footprints. Next to that, the healthcare sector is growing rapidly. This is the consequence of ageing populations,



new developing markets and population expansion [13].

The amount of waste created per hospital patient per day illustrates the severity of this problem. Whereas patients in Mauritius generate only 0.44 kg of waste per day, the patients in the US generate about 8.4 kg [13]. Next to the environmental burden, medical waste also presents a health risk through reinfection. In a report on toxics and human rights, the UN stated that more than half of the world's population is at risk of contracting a healthcare waste related infection [14].

## 1.4 Uniformly distributed clamping

In the past few years, several medtech companies have started to launch state-of-the-art vessel sealers that have been marketed especially for their even distribution of pressure. This sudden need has been kindled by several studies. Lether wrote a literature review looking at factors that affect the seal's performance. Apart from an ideal clamping pressure, he also concluded that the seal is at its best when the clamping pressure is exerted in a uniform manner [3]. Reyes et al. performed a study on the burst pressure (BP) of ex vivo sheep arteries under different sealing conditions. The burst pressure is the pressure at which a seal fails. They found that variations in the applied compression force affected the seal strength. The most beneficial configuration turned out to be a uniformly distributed clamping pressure along the entire jaw length [1]. Voegele et al. concluded the same and added that the jaws should close perpendicularly to the vessel to form the shortest possible seal length [2].

The current standard in bipolar vessel sealing devices is a scissor-like clamp. This is the most accessible shape to introduce to surgeons as it resembles a regular pair of forceps. The problem with this shape is that it distributes the pressure on the tissue unevenly. Because the jaws occlude at an angle, pressure is higher at the proximal (hinge) side and decreases towards the tip. This means that the seal quality (BP) is not consistent across the length of the seal. Figure 3 illustrates this uneven pressure profile.

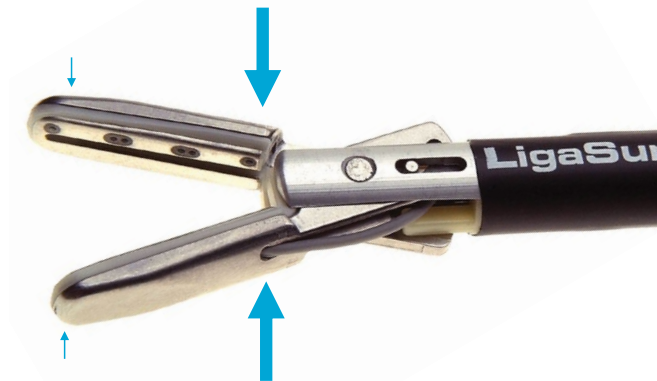


Figure 3: In a scissor clamp, the pressure on the tissue is much higher at the hinge side than at the tip, resulting in an uneven pressure distribution and an inconsistent seal.

## 1.5 Problem definition

### 1.5.1 Reusable bipolar vessel sealer

The problems described above give rise to the need for a reusable BVS device. Half of this thesis is dedicated to the design, development and validation of a reusable laparoscopic bipolar vessel sealer.

It is important to fully clarify what is meant by "reusable". There are tests to prove that

a device is sterile after a full cleaning and sterilisation cycle, but the right resources were lacking for this thesis. To perform this type of test, the final product would have to be fabricated entirely in the right scale, being the 5 mm outer diameter. As this is not going to happen for this thesis, the term "more reusable" is more suitable for the innovation that is going to take place. It is going to be a change in the direction of enhanced cleanability or modularity.

### 1.5.2 Uniform compression

The second purpose of this thesis is to redesign the bipolar vessel sealer so that it distributes the clamping pressure more evenly and that it is capable of making more consistent seals.

### 1.5.3 Area of innovation

The conventional BVS devices generally consist of a tip, a shaft and the handle with the trigger to actuate the sealing mechanism. For the problem of nonuniform pressure distribution, the choice of area of innovation was straightforward, as the tip is the only part that actually touches the tissue to be sealed hence the only part to be able to influence pressure distribution. For the same reason, the choice for innovating in the tip was also made for reusability. The tip is the part that has most contact with tissue and bodily fluids, so a redesign here would greatly improve cleanability. Furthermore, the tip as it is in conventional BVS devices contains a fair amount of occlusion mechanisms and tiny parts, hindering cleanability.

## 1.6 Design goal

The design goal states:

**“Design a state-of-the-art reusable bipolar vessel sealer that can be cleaned along with other surgical equipment due to a modular architecture and that applies a more uniformly distributed pressure to the tissue, improving its performance and making it suitable for use in LMICs.”**

## 1.7 Design requirements

A list of design requirements was made throughout the entire thesis project. The requirements were based on field research, literature, laparoscopy conventions and logical choices regarding the product that was going to be designed.

### The device should...

1. be able to seal blood vessels.
  - (a) prevent leakage of electricity by the use of insulating coatings.
  - (b) seal blood vessels up to 7 mm.
  - (c) grasp and manipulate tissue.
  - (d) be able to divide the tissue with a blade.
  - (e) have straight jaws.
2. be cleanable and sterilisable.
  - (a) be modular.
    - i. not rely on electrical wires for transport of energy to the tip.
    - ii. allow disassembly.
      - A. have a low number of modular parts.
      - B. have clear use cues on how to disassemble.
      - C. have a maximum of two moving parts per clamping jaw.

- iii. allow access throughout the entire shaft (open lumen for cleaning).
  - iv. have a fully removable blade.
- (b) have a mechanism made of surgical steel.
  - (c) rely on a compliant mechanism.
  - (d) distribute the pressure on just one jaw.
  - (e) have a more cleanable hinge than conventional BVS devices.
3. be reusable.
    - (a) perform jaw occlusion and tissue dissection with just one actuation.
    - (b) withstand forces that are exerted on the device by surgical use and cleaning.
    - (c) allow for replacement of modular parts.
  4. exert a uniformly distributed pressure of  $800 \text{ mN/mm}^2$  to the tissue throughout the entire clamping process.
    - (a) allow for adaptation to surface irregularities of  $\pm 0.5 \text{ mm}$ .
    - (b) allow for mechanism distortions up to 6 degrees.
    - (c) use a shape-adaptive approach to clamp the tissue.
  5. adhere to the dimensions for laparoscopic instruments.
    - (a) have an outer diameter of 5 mm.
    - (b) have a shaft + tip length of more than 33 cm.
    - (c) have a seal length of 20 mm.
  6. be safe.
    - (a) not contain any sharp edges that could damage the surroundings.
    - (b) be constructed of biocompatible materials.

## 1.8 Design methodology

After analysis of the problems, different steps were taken to reach the final product. The different design phases can be divided into four categories, being the analysis phase, the conceptual design phase, the experimental validation phase and the embodiment design phase. The different phases can be seen in figure 4.

The design process started with the analysis phase. As this thesis tackles two major problems in bipolar vessel sealing, both analyses had to be performed separately. The analysis phase consisted of finding background information, reading literature and analysing products that are currently available on the market. After the problems were clearly defined, the design goal was constructed and the design methodology was established.

The conceptual phase was less mapped out than the analysis phase. It started with the fuzzy front end of two broad problems. The main choice was what aspect of the product would be leading the synthesis of the innovations. This started a search for product parts or working principles that were causing the problems. Once these fields were isolated, the project scope was narrowed down and solutions could be generated. This was done during the ideation process, in which many concepts were generated and cancelled out until only a few remained.

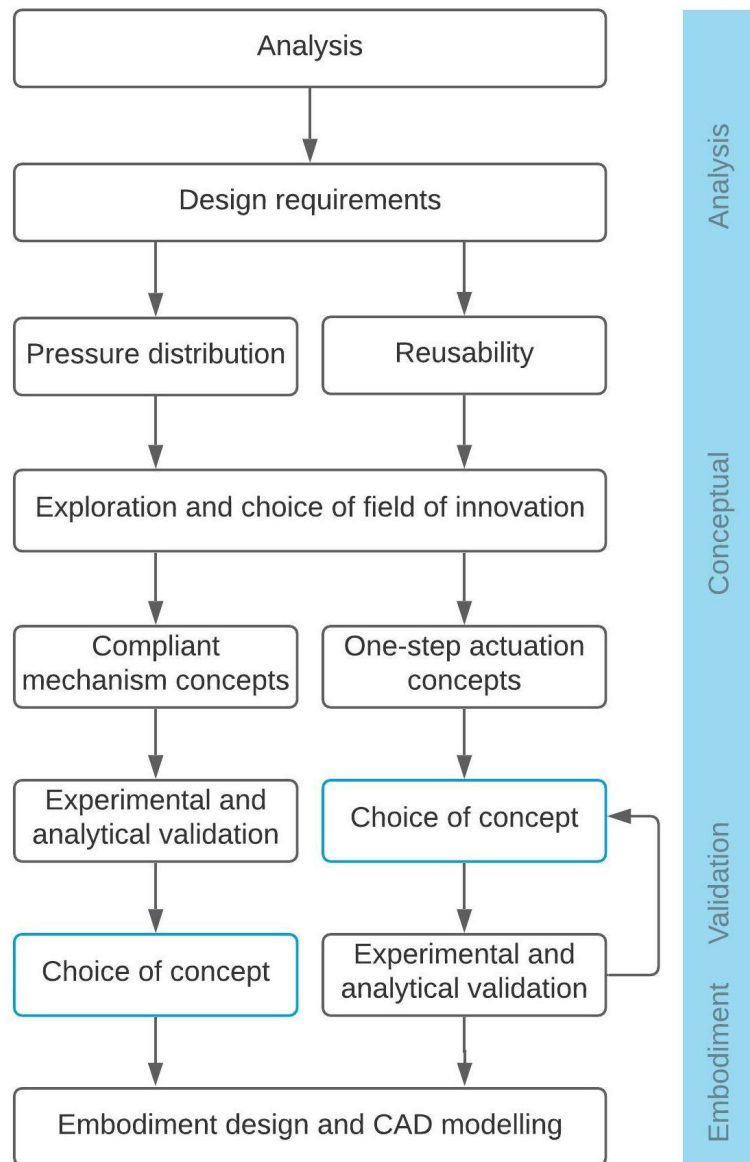


Figure 4: Schematic overview of the four phases of the design process.

The validation phase was performed differently in both problems. In the case of pressure distribution, the validation experiment was used to determine which distribution mechanism works best and is most suitable for the product. The outcome led the decision making process to decide on the winning mechanism. The solution for reusability was already chosen during the conceptual phase. The validation consisted of a physical feasibility test as well as an analytical force analysis for dimensioning. The results of both validation steps were finally evaluated and the final solutions were chosen. Figure 5 shows a detailed illustration of the steps that were taken during this phase.

The final step was the embodiment of the final product. This included shaping the innovated elements into the full assembly, as well as thinking of new innovations to further support cleanability. This was done using SolidWorks. The final product was also delivered in CAD. Only the mechanisms to be tested experimentally were manufactured.

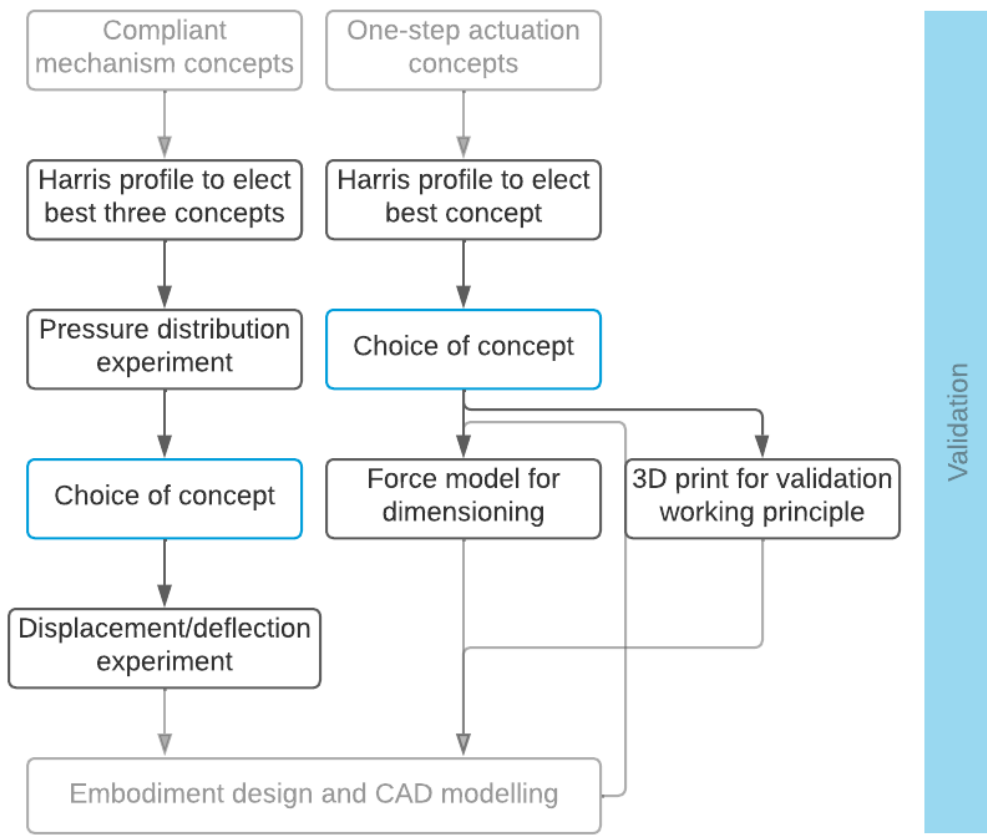


Figure 5: More detailed overview of the validation phase.

## 1.9 Function analyses

For this project, two function analyses were performed: one analysing the conventional bipolar vessel sealing device and one analysing the "future product", i.e. the product to be designed. Figure 43 shows the traditional BVS and figure 44 shows the BVS to be designed with its desired functions. The main takeaway is that the use cycle of a reusable BVS device extends outside the OR. This is the phase in which the device is disassembled, autoclaved, reassembled and packaged for use. Both analyses can be found in the appendix.

## 2 Concept design: reusability

There are two sections describing the concept design phase: one describing the ideation and conceptualisation for reusability and one describing the same process for pressure distribution. The conceptualisation phases have been fueled by identical brainstorming and decision making methods. Ideas have been generated using the "How can I?"-brainstorming method and decisions have been made using Harris' profiles.

### 2.1 Choice of area of innovation

The project had to be narrowed down to a specific part of the product in which the innovation would take place. The hinge is one of the areas in the conventional vessel sealing devices that are hard-to-reach, making the device unsuitable for proper cleaning and sterilisation. This part, together with other design choices, makes the device disposable in most cases. The focus area for innovation has become the hinge or "closing mechanism". If it were possible to reinvent the hinge so that it could be pronounced "more cleanable", the need for redesign on reusability would be satisfied.

#### 2.1.1 Market research hinge

Many manufacturers use different jaw closing mechanisms and they are usually not explicit about the reason behind their choices. A small overview of different hinges can be seen in figure 6. As can be seen in the drawings, a clear distinction can be made between the different closing mechanisms on the market. Some have two moving jaws that actually close like a pair of scissors and some have one stationary (bottom) jaw that does not perform any occluding action.

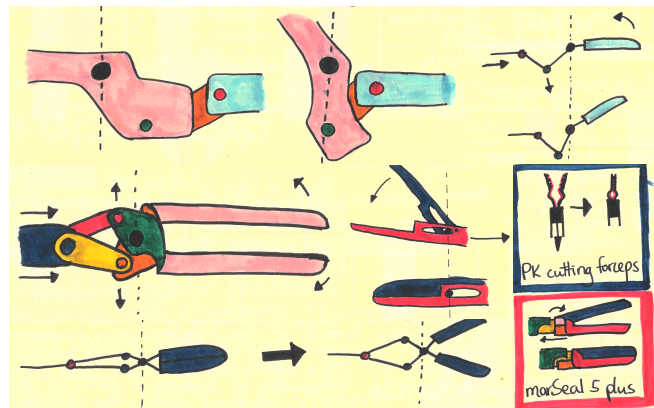


Figure 6: Different hinges that were found during the market research.

The decision was made that the redesigned bipolar vessel sealing device will have one stationary jaw and one jaw that performs all the occluding motion. This configuration was found beneficial for several reasons:

- The blade can easily be deployed as it is always aligned with the shaft.
- Single-jaw occlusion usually requires a hinge with less parts or links. This aligns with the goal of keeping the amount of product parts low for cleanability.
- A simpler hinge could facilitate an easier innovation.

The insight that quickly took lead was one-step actuation of the blade and jaw, inspired by the Detachable Steerable Clip Applier for Dissection of ITA Branches by Alekzander Hoogeweegen [15]. This principle means that the occlusion of the upper jaw and the blade are performed by

one single part. Designing a system as such would mean that at least one part can be taken out of the bipolar vessel sealer, making it more cleanable hence more reusable. Another significant advantage of one-step actuation of the blade and jaw is that a system as such can prevent unnecessary damage to tissues. Automatic occlusion of the jaws when the blade is actuated means that the blade can only be deployed when the jaws are fully occluded, hence it can only dissect the tissue that is being clamped. In other BVS devices like the PK cutting forceps by Olympus, accidental actuation of the blade with open jaws is possible, leaving the surgeon at risk of slashing the blade through surrounding tissues.

## 2.2 Choice of innovation

The blade slit mechanism is a concept in which an extension of the upper jaw slides through a cutout profile in the blade when the blade is deployed. The shape of this profile causes the upper jaw to close during the initial displacement of the blade. Continued displacement allows the blade to slide to the tip and dissect sealed tissue. Figure 8 shows an illustration of the concept in its infancy.

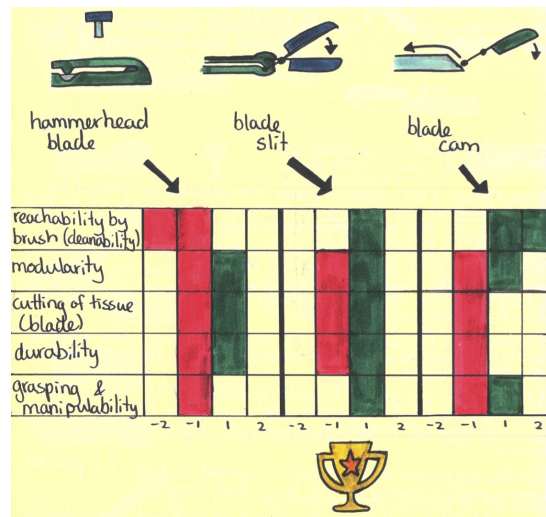


Figure 7: Harris profile electing the "blade slit" as winning working principle for reusability.

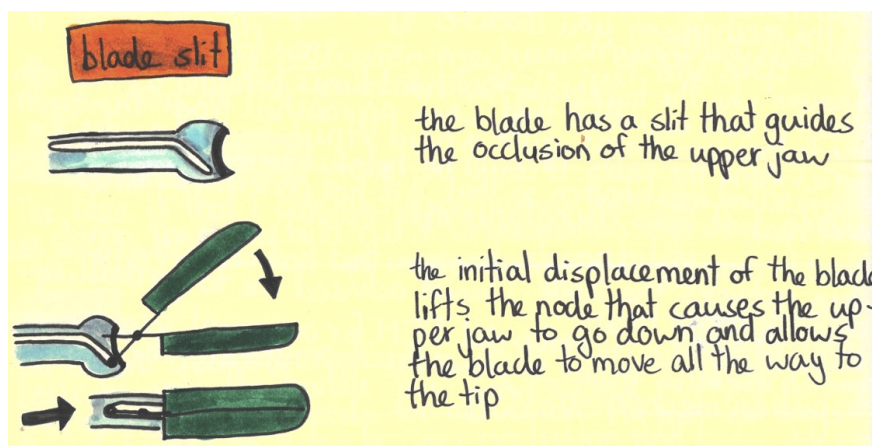


Figure 8: A log book snippet explaining the blade slit concept.

### 3 Concept design: pressure distribution

As several studies have shown that a uniform pressure profile promotes the quality of the seal (BP), it is desirable to design a mechanism that facilitates this. The coming section is entitled to the conceptualisation journey that ends in the selection of three possible mechanisms that will be tested later during the validation phase.

#### 3.1 Choice of type of mechanism

The search for what type of mechanism could become useful for pressure distribution in BVS devices started with a diverging phase in which principles for pressure distribution were gathered.

##### 3.1.1 Literature studies

Prior to this thesis, a literature study was performed with the title: "Mechanisms to achieve a Uniformly Distributed Pressure across a Clamped Surface". This study was performed to prepare for this thesis by gaining insight in possible solutions. There were 23 articles that were found to be relevant. These articles contained mechanisms that had the main purpose of uniformly distributing clamping pressure. They were selected by analysis of the working principles and visual comparison to see what could be suitable for use in BVS devices. The search extended beyond the medical field, so the mechanisms had applications in all kinds of industries. The outcome comprised six mechanisms that could be suitable for vessel sealing. Half of them consists of clamps in which the jaws approach each other in a parallel fashion and the other half consists of circular clamps that inflate inwards to clamp the object. Finally, three mechanisms were found to possibly be suitable for application in bipolar vessel sealing looking at the force they can exert. The conclusion was drawn that circumferentially shrinking clamps are less convenient for use in bipolar vessel sealing, so the parallel clamps were elected most suitable [16].

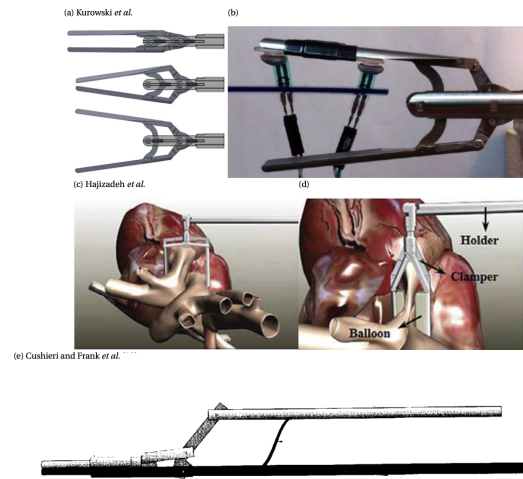


Figure 9: The three mechanisms from the literature review that turned out to be most suitable for use in bipolar vessel sealing. From top to bottom: lung tumour localisation device by Kurowski et al. (image a and b), the aortic cross-clamp by Hajizadeh Farkoush et al. (image c and d) and the detachable parallel action clamp by Cuschieri and Frank (image e) [17][18][19].

This literature review served as a source of inspiration for the problems of uniform distribution of clamping pressure in bipolar vessel sealing.



### 3.1.2 Market research pressure distribution

A market research was performed to get a feeling of how manufacturers handle the problems of cleanability and pressure distribution in their existing bipolar vessel sealers. Most BVS devices are disposable because it takes extra development steps and companies earn more on disposables on the long run [20]. Some companies do offer reusable BVS devices, but these are generally costly and too expensive for use in LMICs. Examples of reusable vessel sealers are the marSeal5 plus by KLS Martin and the Thermocut by Lamidey Noury. Apart from the blade, these devices are fully reusable.

Medtronic's LigaSure, one of the market leaders in bipolar vessel sealers, only produces devices with the traditional scissor-like clamping configuration. This results in pressure peaks near the hinge and hardly no pressure near the tip (figure 40 in the appendix). Companies like Ethicon (ENSEAL G2) and B. Braun (Caiman 5) sell BVS devices with unique built-in mechanisms to promote pressure distribution. ENSEAL G2 uses its I-shaped blade to ensure constant compression from the hinge to the tip and Caiman 5 has an extra hinge in the bottom jaw for tip-first closure and a parallel occluding upper jaw for pressure distribution.

### 3.1.3 Choice of principle

After performing a pressure-cooker design of one of the principles, research was done to determine the general advantages of the different types of mechanisms. With this knowledge, the final decision was made using the Harris profile method. As can be seen in figure 10, the category of compliant mechanisms was elected as most suitable for our design purposes. This decision was substantiated by the overall simplicity that overshadows the concept of compliance. The main incentive for people to use compliant mechanisms is the dramatic reduction in the total number of parts needed to accomplish a certain task. Looking from a cleanability perspective, having less parts means that it will be easier to disassemble the product and to clean it. Besides this, compliant mechanisms also come with other advantages:

- Facile production processes
- Low price (fewer parts and facile production)
- Precise motion by reducing backlash and wear
- Better performance due to reduced friction
- Ease of miniaturisation (suitable for micromechanisms)
- High level of predictability because the energy is stored in the form of strain energy [21].

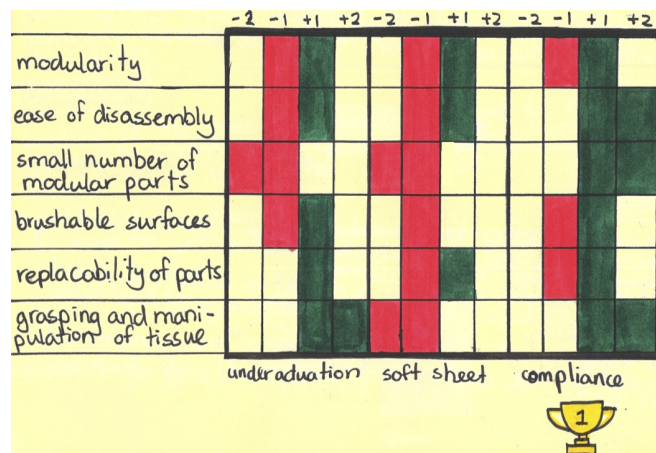


Figure 10: The Harris profile used to determine the type of mechanism to be designed.

## 3.2 Choice of mechanisms

### 3.2.1 Research tissue thickness

It is important to know the average tissue thickness and matter of surface irregularity of the relevant tissue. Knowing this gives insight in how high the resolution of pressure distribution should be. The word resolution is used to indicate the amount of moving articulating parts needed to distribute pressure in a distribution mechanism.

The research was performed by analysis of footage of a total laparoscopic hysterectomy (TLH) in which a LigaSure Maryland device was used. Different film stills were selected for presence of clamping action and the accompanying tissue thickness and surface irregularities. Knowing the dimensions of the LigaSure Maryland, the average tissue thickness and irregularity could be measured and calculated. Figure 11 shows one of the still used for measurements. Knowing the results and of the occurrence of surface irregularities, the conclusion was drawn that, if there would be shape-adaptive media on the clamp's articulating surface, the amount of moving parts should be kept as low as possible, with a maximum of 2.

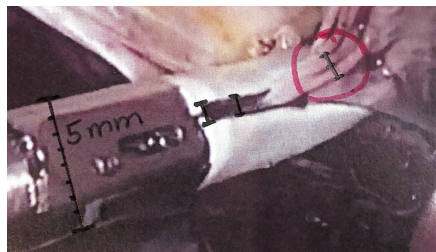


Figure 11: A still used to research average tissue thickness.

### 3.2.2 Assumptions on force, material, dimensions and distortions

Throughout the process of ideation it became more evident that some parameters needed to be determined in order to be able to generate more fitting concepts. A little research was set up and the following findings/assumptions have been gathered:

**Force/pressure** The amount of force or pressure that a BVS device exerts on the tissue is an important factor to take into consideration. While many different BVS devices exert different forces/pressures, there is one study that investigates the optimal sealing pressure. Wallwiener et al. performed experiments on 239 renal arteries from commercially slaughtered female pigs. The outcomes of the experiment were seal success (resistance to 250 mmHg intraluminal pressure for 2 min) and seal stability (BP). He found that sealing pressure has a significant impact on seal quality, with 800 mN/mm<sup>2</sup> showing the best sealing results.

**Dimensions** The dimensions of the device generally have to do with the purpose of the clamp, i.e. what kind of tissue it should be able to grasp. Whereas most BVS devices claim to function properly when used on blood vessels up to 7 mm in diameter, other types of tissue can be much larger. The 7 mm constraint has to do with the accompanying blood pressures and vessel wall thicknesses that also have to be overcome by the clamp [22]. If the device would only have to be able to clamp blood vessels up to 7 mm in diameter, that would mean that the jaws would technically seen only need to be around 11 mm long. However, market research shows that most BVS devices have a seal length of around 20 mm, with extremities extending to 26.5 mm. The reason behind this has been clarified through email contact with Roelf Postema, a surgeon at several hospitals throughout the Netherlands. He confirmed that the jaws are generally longer because blood vessels are just one group of tissue for which the devices are used. Apart from arteries and veins, he also uses the device to seal fat tissue and peritoneum. The email can be found in the appendix. From the market research and the

dialogue with doctor Postema, the conclusion has been drawn that a jaw length of 20 mm is a desirable objective to work with. The outer diameter of the system is 5 mm, determined by laparoscopic convention. To play with the inner dimensioning, one idea for a compliant mechanism was adopted and drawn out. This approximation provided the the basis for the calculation of the distortion/warp the mechanism will be subjected to and can be seen in figure 12.

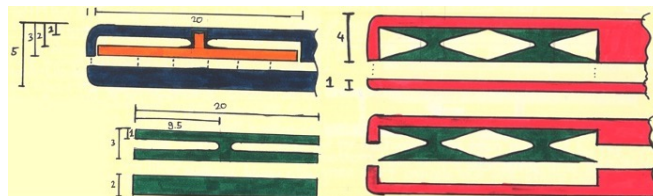


Figure 12: A set of tryouts for tweaking the inner dimensions of the tip.

**Material used** The material to be used is surgical steel, as this is conventional in surgical equipment. Surgical steel has no formal definition, but commonly accepted types include austenitic 316 stainless and martensitic 440 and 420 stainless [23].

**Distortion/warp** The distortion or warp that the mechanism will undergo has been derived from the average tissue thickness and average matter of surface irregularity that have been investigated earlier in this section. This information combined with the approximation of inner dimensions provided the basis for warp calculations. Depending on the location of the irregularity, the calculated warp ranges between  $3^\circ$  and  $6^\circ$ .

### 3.2.3 Choice of mechanisms

The next objective was to generate three conceptual compliant mechanisms that could distribute pressure in a bipolar vessel sealing device. To get inspired, several mechanical engineering databases were consulted. These pages display extensive lists of compliant mechanisms and their uses. The three mechanisms that came out of this process are the spring toy, trapezium and leaf spring, listed in order of increasing complexity. The spring toy mechanism can be compared to a compliant seesaw in which the long horizontal beam remains rigid and the short vertical beam performs the deflecting action. This simple design allows the articulating surface to adapt to the tangentiality of the clamped tissue, distributing pressure. The trapezium mechanism has four rigid beams and four deflecting corners. By applying pressure to the shorter horizontal beam, the structure collapses and the articulating surface adapts to the tangentiality of the tissue. Depending on the location of the applied pressure with respect to the center of the articulating surface, the mechanism deflects either left or right. The interesting difference between the articulating surfaces of the trapezium and the spring toy mechanism is the way they move upon deflection. Whereas the spring toy acts like a seesaw, pivoting around a central axis, the trapezium surface also performs a horizontal displacement when interfered with. The third mechanism is the leaf spring. It uses a thin bent steel strip to act like a cushion, encapsulating the geometry of the tissue. This mechanism is considered most complicated as it is unsure in which ways it will deflect and analytical models of deflection are extremely challenging for this case. All three mechanisms can be seen in figure 13.

## 3.3 Model for verification of dimensions

Different models were made to check the feasibility of the mechanism ideas in the current set of dimensions. It was important to investigate whether the systems were able to withstand the required forces on this scale before continuing to work with them. Entering the equations into Excel allowed for tweaking of dimensions and forces. The drawings and equations can be found in the appendix.

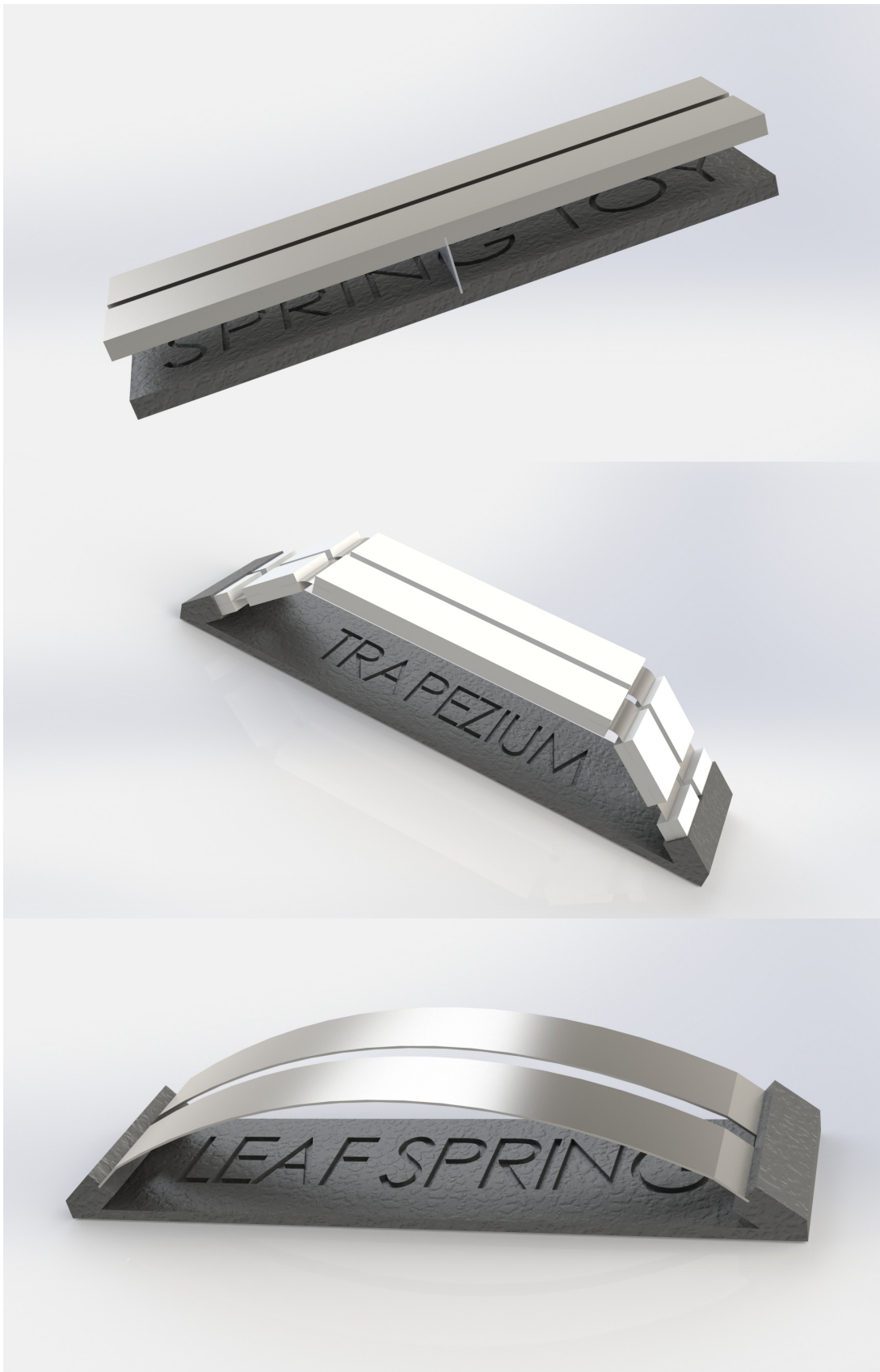


Figure 13: The three distribution mechanisms that will take part in the experiment to find out which will perform best at uniformly distributing pressure in a clamping configuration. From top to bottom: spring toy, trapezium, leaf spring.

## 4 Concept validation

The pressure distribution experiment was executed to test which of the three mechanisms performs best at distributing pressure on tissue. The outcome of the experiment decided which mechanism would be implemented in the final design of the bipolar vessel sealer. A full lab report of the experiment can be found in the appendix.

### 4.1 Methods

The experiment comprised a setup in which a displacement/speed controlled linear stage (Aerotech PRO115-400-UF) caused a piece of phantom tissue (Ecoflex 00-50 silicon) to collide into one of the distribution mechanisms. This happened at a total force of  $7\pm 0.1$  N, a value that had been determined earlier using a scale because it showed the right amount of deflection and deformation in the mechanisms and phantoms respectively. Too much force would cause the mechanisms to collide internally and too little force would hinder the mechanisms from showing their pressure distribution capabilities. The linear stage carried the phantom and pushed it upwards against the center of the distribution mechanism. This placement was regulated by pieces of sticky tape on the rigid and sliding parts of the setup.

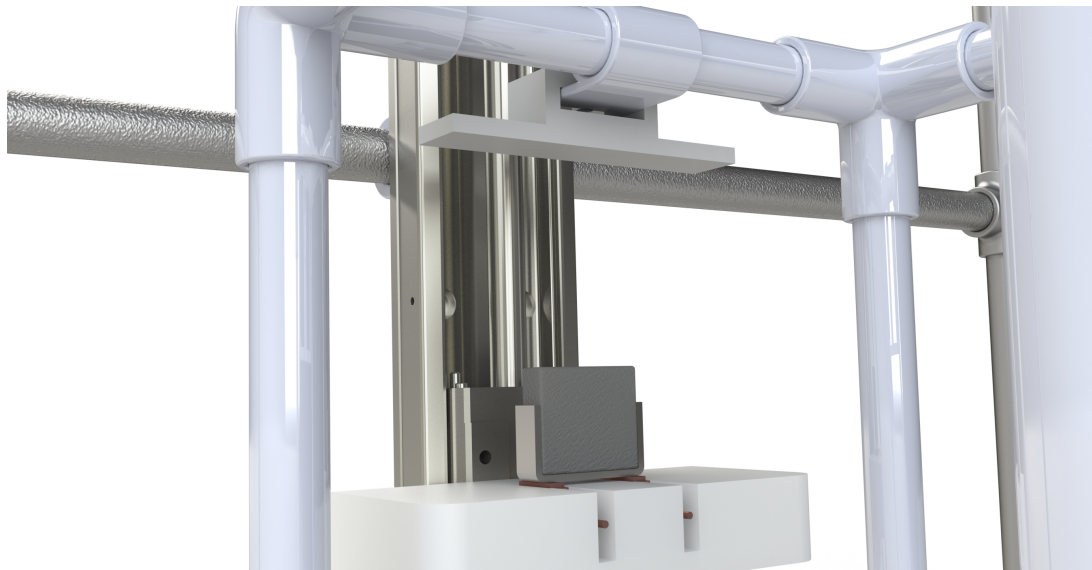


Figure 14: The experiment setup with a flat bar as "mechanism".

The pressure distribution was measured in two ways: through load cells (FUTEK Miniature S-Beam Jr. Load Cell) and through pressure-sensitive film (FujiFilm Prescale 5LW). The phantom support has two holes in the top, each containing a load cell. This can be seen in figure 15. The phantom itself was placed onto a steel sheet which connects to both load cells with a screw. Upon collision with the distribution mechanism, the load cells measured the downward force under the right and left extremes of the phantom. Comparison of these values resulted in the difference of force between the two points,  $\Delta F$ . The closer this  $\Delta F$  was to 0, the more uniform the pressure profile was. Every measurement has been repeated five times. The calibration of the load cells is explained in the appendix.

The current pressure distribution measurement system only measures the forces on either side of the phantom and not in the middle. This means that any irregularities in this 'dead space' go unnoticed, unless another measurement system is added that covers this space. For example, a point load in the middle of the steel plate would be broken down into two equal forces and would give a  $\Delta F$  of 0, whereas in reality the pressure profile is nonuniform. To

make up for this shortcoming, pressure-sensitive film was placed between the phantom and the steel plate. This film changes colour when compressed. The uniformity can be determined by looking at the film, in the sense that homogeneity in colour means uniform and heterogeneity means nonuniform pressure.

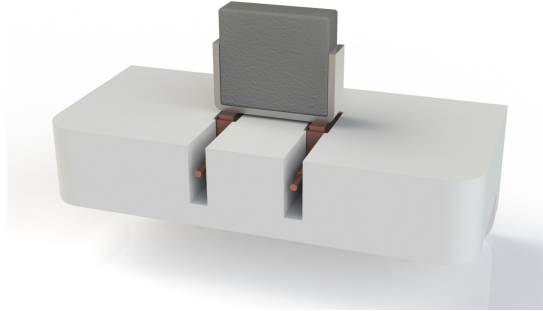


Figure 15: The phantom support showing the FUTEK load cells and the steel plate holding the phantom.

#### 4.1.1 Experimental variables

Looking at the mechanisms tested in the experiment, four variables were tested, being the control mechanism and the three compliant mechanisms. The control mechanism was made to mimic the conventional BVS clamping situation. This was done by pushing the phantoms against a rigid beam that had an inclination of  $35^\circ$ . Comparison of the control results with the results of the three mechanisms would show whether the newly designed distribution mechanisms outperform the conventional situation, hence improve the pressure distribution.

The experiment was initially performed using three silicon phantom tissue shapes, being the peak, the flat and the round sample. This variation in shapes was used so that the mechanisms could be tested with different surface geometries. The phantoms can be seen in figure 16. Every mechanism/phantom combination was tested five times. Figure 16 also shows a fourth phantom which was not used initially. The paragraph below clarifies this.

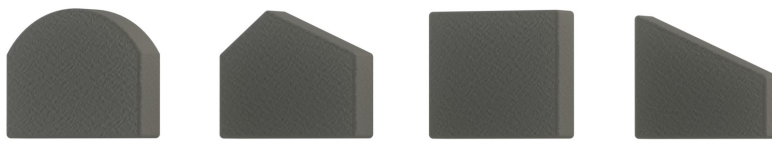


Figure 16: The four silicon phantoms that were used during the experiment. From left to right: round, peak, flat, incline.

Later evaluation of the executed experiment led to the insight that the results would be more valuable if the mechanism was placed at a slight angle. This is because the jaws occlude like a pair of scissors. Unless tissue thickness is infinitesimally small, the upper jaw will never hit the tissue in a parallel fashion. The decision was made that the experiment would be repeated at an angle for the control mechanism and the mechanism that performed the best. These mechanisms were to be tested with all four phantoms. Additionally, the pressure-sensitive film would be placed on top of the phantom, i.e. at the phantom/mechanism interface. Figure 17 and equation 1 show how the angle was determined using the calculated tissue thickness and the length of the jaws. The assumption was made that the tissue is clamped at half the length of the jaw.

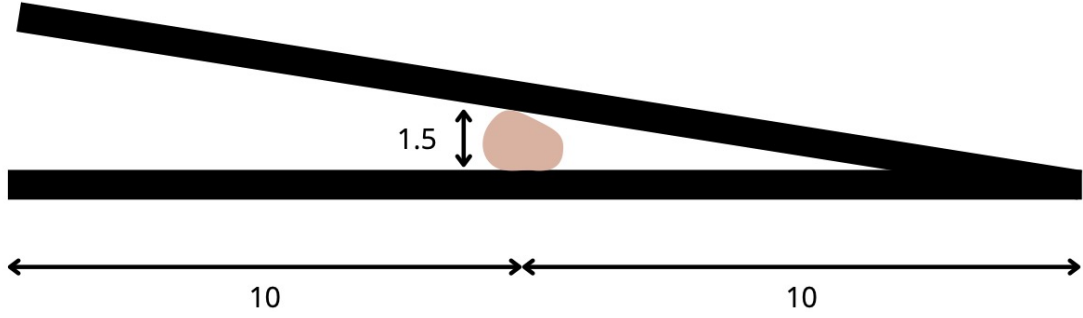


Figure 17: Illustration showing the how the angle of  $8.5^\circ$  was determined. Equation 1 shows the calculation.

$$\arctan(1.5/10) \approx 8.5^\circ \quad (1)$$

Figure 18 shows the new setup with the leaf spring mechanism and the control mechanism at an inclination of  $8.5^\circ$ . An important thing that changed when the mechanism was put at an angle is that the system cannot be considered symmetrical anymore. Therefore, experiments with the peak and incline phantom have been carried out twice; once in every orientation. The average of these values has been calculated and was used for further data processing.

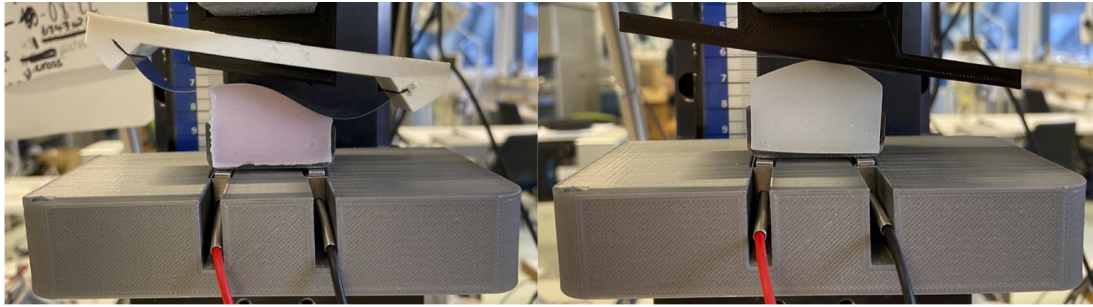


Figure 18: The added experiment setup with the leaf spring (left) and the control mechanism (right) at an angle of  $8.5^\circ$ .

## 4.2 Processing of data

LabVIEW 2018 was used to read out the sensor values for every 100 ms and to keep track of the sum of the two. This was important to assure that the total force of  $7 \pm 0.1$  N was applied in every measurement, making the values fit for comparison. Excel was used to plot the results. The  $\Delta F$  was determined by taking the absolute difference between the two force values of the latest time frame that measured a total force of  $7 \pm 0.1$  N (equation 2). Figure 19 shows one of the graphs containing the sensor values and the total force (N) over time (ms). The typical measurement points used for determination of  $\Delta F$  have been indicated with black circles.

$$\Delta F = |F_{left} - F_{right}| \quad (2)$$

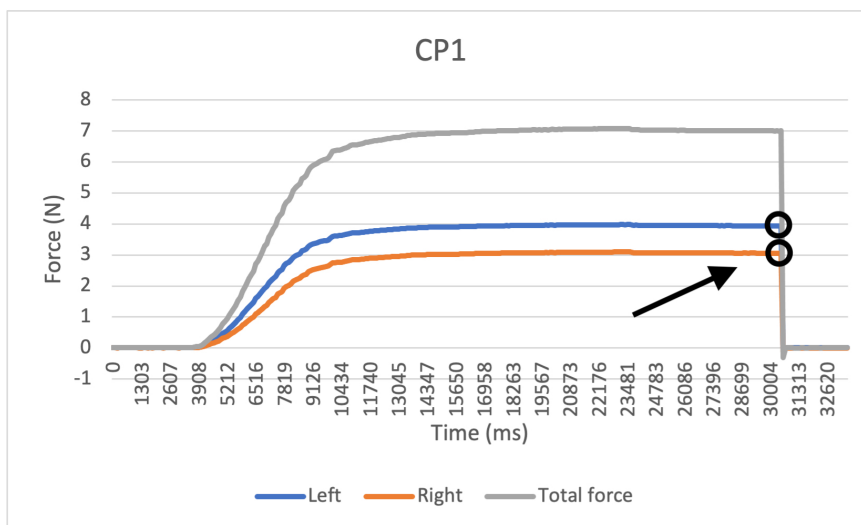


Figure 19: A plot showing both sensor values (N) and the total force over time (ms). The circles show the two measurement points used to determine  $\Delta F$ .

### 4.3 Validity of load cells for force measurement

An important thing to investigate was the validity of using load cells for pressure distribution measurements. This was examined by comparison of a number of predictable situations. Imagine the spring toy approaching a perfectly rectangular phantom, like in figure 20. The only force acting on the load cells is a vertical downward force, i.e. the only force the load cell can measure. In this situation, it is clear that the load cells measure the desired information, being compression forces.

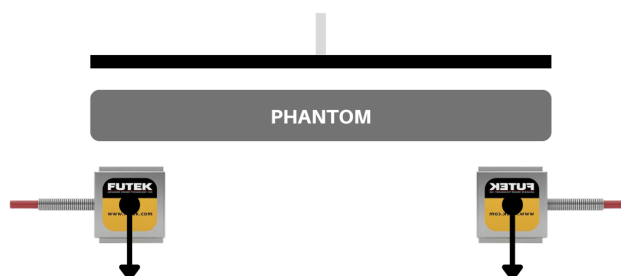


Figure 20: Spring toy exerting pressure to a rectangular phantom.

Now imagine a situation in which the spring toy approaches a phantom that has a diagonal upper surface. Applying downward pressure now does not just result in a downward force on the load cells, but also a shear force at  $90^\circ$  relative to the downward force. The situation can be seen in figure 21. The load cells can only measure the compression forces, not the shear forces.

The force exerted by the spring toy in diagonal position is perpendicular to the diagonal surface. This force can be broken down in a vertical and a horizontal component, the former being the compression force and the latter the shear force. As long as the inclination of the articulating surface of the distribution mechanism remains constant across its length, the part of the clamping force that turns into a horizontal force is constant across the phantom's surface. This means that, when investigating (differential) pressure distribution and not quantitative



pressure values, the compression forces measured on each load cell form a reliable medium for comparison to gain insight in pressure uniformity.

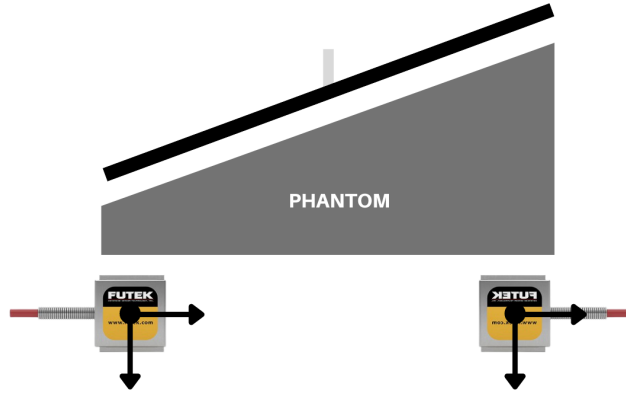


Figure 21: Spring toy exerting pressure to a phantom with a diagonal surface.

## 4.4 Results

The  $\Delta F$  of every (no incline) measurement was listed and the average value of each mechanism/phantom combination was calculated. The values are displayed in table 6 in the appendix. To get a better overview of the total performance of each mechanism, the average values of each mechanism/phantom combination were listed in table 1 and the average  $\Delta F$  per mechanism was calculated from this. This number represents the average performance of one specific mechanism with all three phantoms. Table 1 shows that the leaf spring has the best overall performance (lowest  $\Delta F$ ), followed by the spring toy, the control mechanism and the trapezium. The pressure-sensitive film showed no reproducible pressure hot spots or abnormalities. A scan of the leaf spring films can be found in figure 54 the appendix.

	Control	Leaf spring	Spring toy	Trapezium
<b>Peak</b>	0.8974	0.5042	2.2522	0.3538
<b>Flat</b>	0.402	0.3078	0.2022	6.926
<b>Round</b>	2.8538	0.9272	1.285	1.6298
<b>AVG</b>	<b>1.38</b>	<b>0.58</b>	<b>1.25</b>	<b>2.97</b>

Table 1: The average  $\Delta F$  (N) per mechanism. The leaf spring stands out with the lowest value.

### 4.4.1 Results angle experiment

The numerical results of the extra load cell measurements at an inclination of  $8.5^\circ$  can be seen in table 2 and 3. The "true averages" have been calculated by first taking the average of the double measurements for asymmetrical phantoms and then treating this number as if it were one measurement. Without doing so, the asymmetrical phantoms would have twice the weight in the average compared to symmetrical phantoms. The conclusion can be drawn that, looking at the load cell measurements, the control mechanism outperforms the leaf spring mechanism at an inclination of  $8.5^\circ$ . The results of the pressure-sensitive film measurements can be seen in figures 56 and 57 in the appendix.

	<b>1</b>	<b>2</b>	<b>3</b>	<b>4</b>	<b>5</b>	<b>AVG</b>	<b>TRUE AVG</b>
<b>LSR</b>	1.674	1.619	1.629	1.633	1.647	<b>1.64</b>	<b>1.64</b>
<b>LSF</b>	2.101	2.105	2.11	2.11	2.11	<b>2.11</b>	<b>2.11</b>
<b>LSPL</b>	1.096	1.091	1.087	1.087	1.073	<b>1.09</b>	<b>0.86</b>
<b>LSPR</b>	0.633	0.632	0.623	0.619	0.623	<b>0.63</b>	
<b>LSIL</b>	0.87	0.889	0.82	0.769	0.821	<b>0.83</b>	<b>0.69</b>
<b>LSIR</b>	0.558	0.55	0.55	0.558	0.55	<b>0.55</b>	
						<b>1.14</b>	<b>1.32</b>

Table 2: The results of the additional experiment. The table shows the  $\Delta F$  of the leaf spring (at an angle) with all four phantoms. From top to bottom: round, flat, peak (left), peak (right), incline (left), incline (right).

	<b>1</b>	<b>2</b>	<b>3</b>	<b>4</b>	<b>5</b>	<b>AVG</b>	<b>TRUE AVG</b>
<b>CR</b>	0.225	0.248	0.248	0.244	0.243	<b>0.24</b>	<b>0.24</b>
<b>CF</b>	0.008	0.013	0.014	0.014	0.017	<b>0.01</b>	<b>0.01</b>
<b>CPL</b>	1.729	1.711	1.711	1.71	1.711	<b>1.71</b>	<b>1.22</b>
<b>CPR</b>	0.728	0.738	0.738	0.72	0.692	<b>0.72</b>	
<b>CIR</b>	1.097	0.895	0.909	0.9	0.895	<b>0.94</b>	<b>1.66</b>
<b>CIL</b>	2.39	2.385	2.39	2.389	2.399	<b>2.39</b>	
						<b>1.00</b>	<b>0.78</b>

Table 3: The results of the additional experiment. The table shows the  $\Delta F$  of the control mechanism (at an angle) with all four phantoms. From top to bottom: round, flat, peak (left), peak (right), incline (left), incline (right).

## 4.5 Discussion

Looking at table 1, the conclusion could be drawn that the leaf spring mechanism has the average best performance in terms of  $\Delta F$ . This mechanism however was not the best in with every mechanism/phantom combination, as there were situations in which other mechanisms outperformed the leaf spring (table 1). This subsection will elaborate on the superior performance of the leaf spring, discuss some remarkable results and possible shortcomings of the experiment.

### 4.5.1 Explanation of results

Figure 24 shows pictures of the cases discussed to support the understanding.

**Control/round/flat** In all cases, the control mechanism was positioned in a way that the right part would hit the phantom before the left part did (picture 1 and 2 in figure 24). Intuitively, one would expect the right load cell to measure more force than the left load cell, as the right part is being pushed down more relative to the left part. However, in all measurements with the control condition, the left load cell measured the most force. The  $\Delta F$  was greatest when using the round phantom. Figure 22 shows the situation. Instead of mainly compressing the right part, the control mechanism seems to push the material to the left side, causing a shift in volume. The right half of figure 22 shows the deformation the phantom undergoes when compressed by the control mechanism. Note how the material shift to the left even increases the height of the phantom in this side.

The control mechanism performs better on the flat phantom. Like with the round phantom, the left load cell measures more force, but the difference between left and right is smaller. The conclusion can be drawn that this difference is due to the shape of the phantom. Figure

23 shows the deformation the flat phantom undergoes when compressed by the control mechanism. Comparing the right image to that of figure 22, it can be observed that more material on the right side is being pushed down than in the control/round combination (larger grey plane).

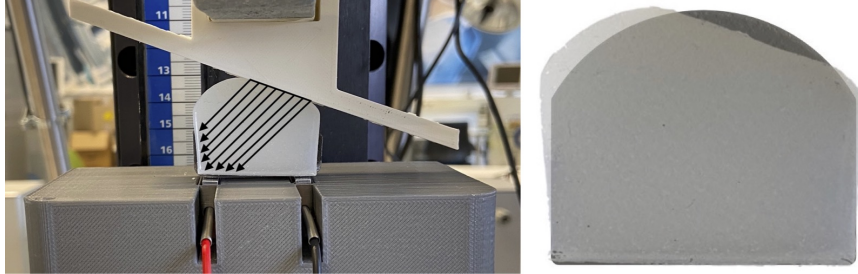


Figure 22: The clamping situation with the control mechanism (left) and the deformation of the round phantom when compressed by the control mechanism (right).

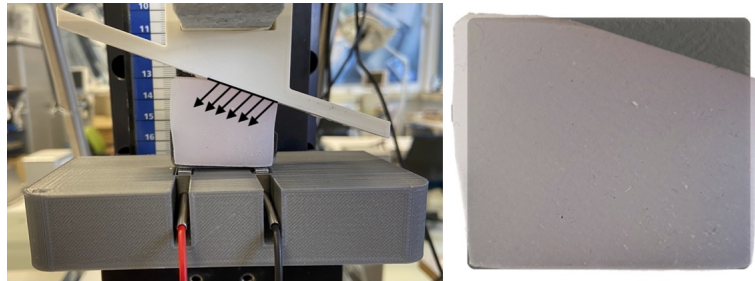


Figure 23: The clamping situation with the control mechanism (left) and the deformation of the flat phantom when compressed by the control mechanism (right).

**Spring toy/peak/flat** The spring toy/peak combination shows poor results. This is due to the central placement of the phantom against the mechanism. All experiments were conducted in a way that the phantom approached the mechanism right in the center. Figure 48 in the appendix shows an analytical model of the deflection of the spring toy mechanism. To bend the vertical beam, a certain moment  $M_a$  needs to be applied. This moment is induced by vertical force  $F_n$  and arm  $r_n$ . In the case of the spring toy/peak combination, the location of  $F_n$  is so close to pivot point A ( $r_n$  is small) that it exerts too little force to bend the mechanism. This results in the mechanism not being able to adapt its articulating surface tangentially to the surface of the peak phantom. The situation can be seen in image 6 in figure 24 in the appendix. When the spring toy does not adjust its tangentiality to the clamped surface, it ends up functioning like a parallel occluding clamp.

This also explains why the spring toy/flat combination (figure 24 image 5) gave such good distribution results, as there are two flat surfaces pushing against each other. Because this situation seems unfair, another side experiment was conducted in which the flat and peak phantom were positioned off-centered. These situations can be seen in figure 55 in the appendix. The flat phantom shows expected results, as a deflected spring toy means that an inclined surface is pushing against a flat surface. The peak phantom also showed inferior results. This is because the spring toy surface could not match the tangentiality of the peak phantom with this amount of total force applied. It can be concluded that for both cases, centered placement of the phantom gives a more uniform distribution of pressure.

**Trapezium/peak/flat** When in collision with the peak phantom (image 3 in figure 24), the articulating beam of the trapezium mechanism tilted and translated to the right to suit the phantom's tangentiality. This combination resulted in a low  $\Delta F$  and was the mechanism's best performance. However, something unforeseen occurred when the trapezium mechanism was combined with the flat phantom. The collision can be seen in figure 24 image 4. The problem is that the articulating beam of the trapezium mechanism can only stay horizontal when the force applied by the phantom is positioned perfectly in the middle of the beam. Whenever this force is (slightly) off-centered, the trapezium mechanism will pick that side and will fully deflect in that direction. This leaves the trapezium/flat combination highly unsuitable as it delivered the worst distribution results of the experiment. Especially concerning the fact that this phenomenon occurs only with the flat phantom, which is assumed the "safest" condition. We can conclude that the trapezium mechanism only distributes pressure when collided with surface irregularities.

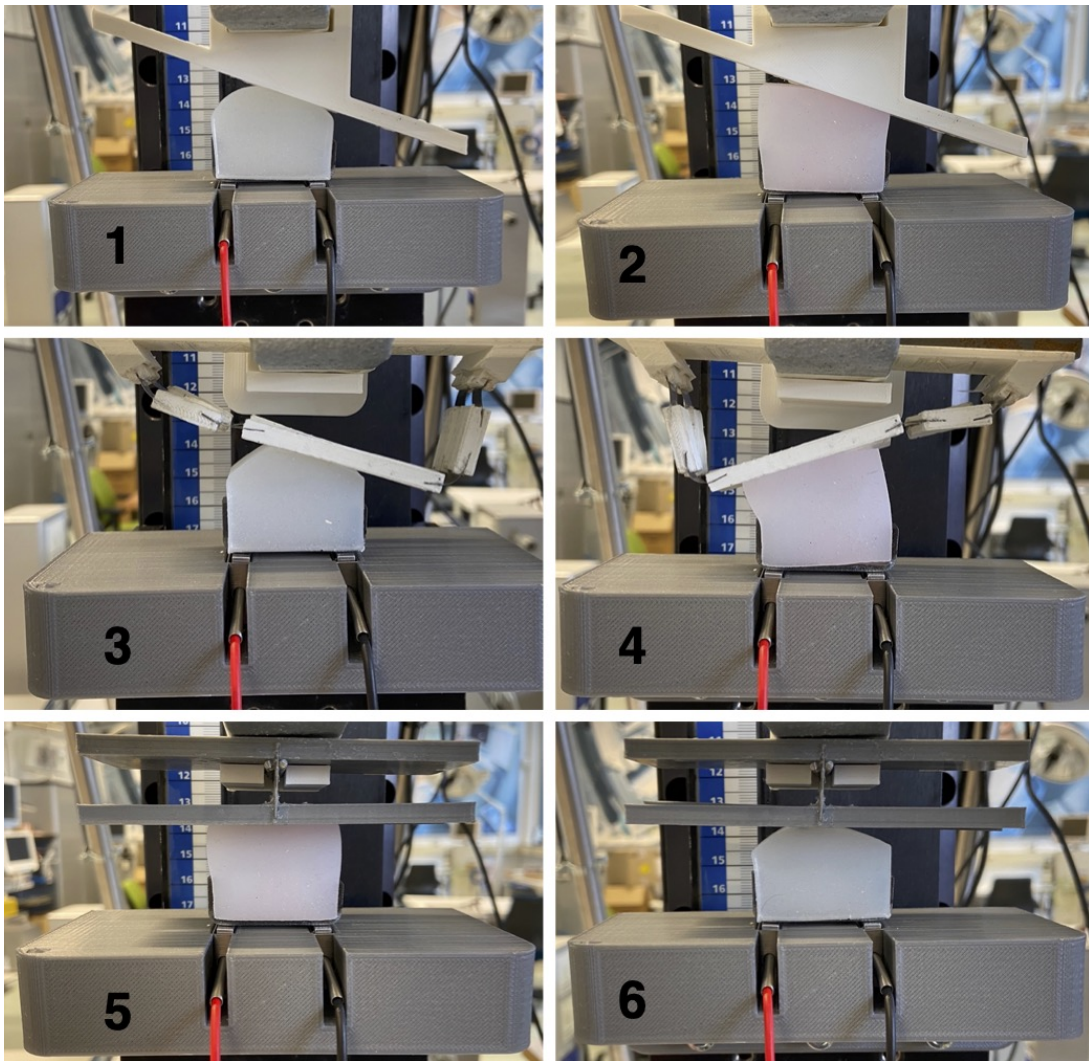


Figure 24: Results of experiment with the other three mechanisms.

#### 4.5.2 Leaf spring performance

The conclusion could be drawn that the leaf spring mechanism outperformed the other three mechanisms at no inclination looking at the average  $\Delta F$  measured by the load cells. Figure 25 shows pictures of the leaf spring mechanism in interaction with all phantom shapes. Note how

the steel sheet fully adapts to the surface geometry of the phantoms. It is this shape-adaptive capability what makes the leaf spring mechanism outperform the other mechanisms looking at the average  $\Delta F$ . The three cases in which the other mechanisms outperformed the leaf spring were all situations in which the articulating surface of the mechanism could perfectly align tangentially to the surface of the phantom. This was only possible with interaction between flat surfaces. Looking at the results of the round phantom in table 1, one can see that the other (flat) mechanisms underachieve when the tissue sample has a more organic shape. This finding supports the conclusion of the leaf spring mechanism being most fit for use in bipolar vessel sealing, as the tissues a BVS device will clamp will generally deal with organic geometries.

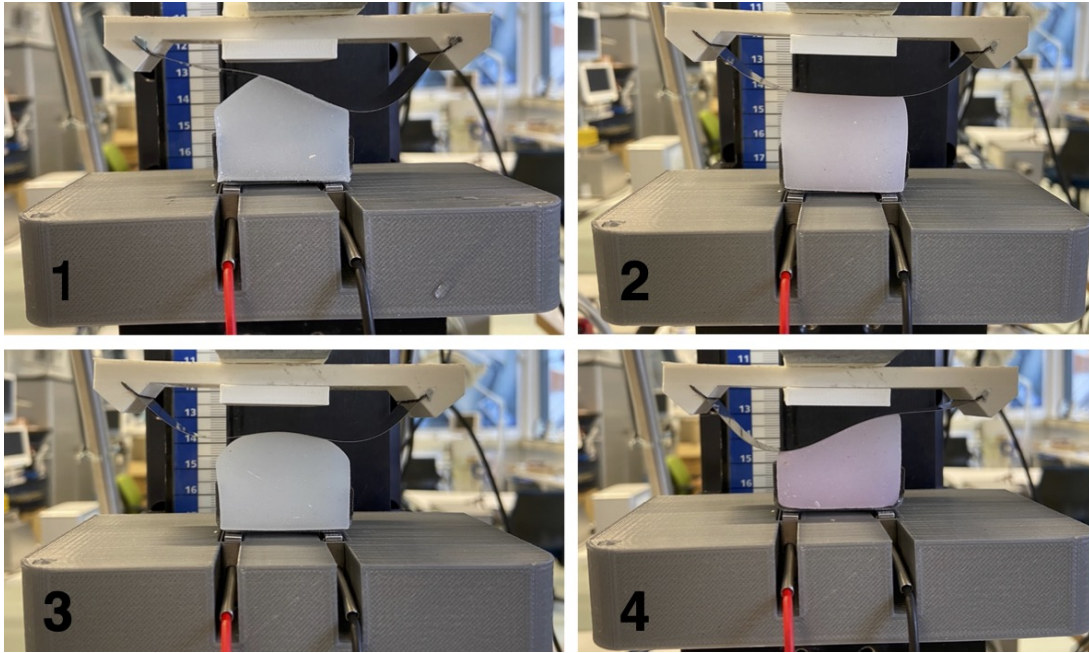


Figure 25: The leaf spring mechanism collided with the four different phantoms.

To further test the feasibility of the use of the leaf spring mechanism for pressure distribution, it was subjected to one last condition: the inclined phantom. This phantom had been experimented with earlier, but was omitted because it seemed to produce illegitimate results. The problem was that the material on the higher side of the phantom was pushed over the edge of the phantom support plate in most cases. Another problem was the asymmetrical nature of the incline phantom. Putting the phantom in one way gave different results compared to the other way. This problem will be discussed further in section 4.5.5. To overcome this discrepancy, both orientations were recorded and the average was taken. Table 4 shows the results of the leaf spring/incline, the control/incline left and the control/incline right combination with the average  $\Delta F$ . We can conclude that the leaf spring mechanism (no incline) performs better at distributing pressure than the average performance of the control mechanism. Figure 26 shows the three combinations in the same order as table 4. It can be observed that the leaf spring was the only mechanism that did not cause the problem of material being pushed over the side. This is due to its unique shape-adaptive capabilities.

	1	2	3	4	5	AVG
<b>LI</b>	0.788	0.751	0.774	0.714	0.72	<b>0.75</b>
<b>CIL</b>	1.609	1.586	1.577	1.582	1.586	<b>1.59</b>
<b>CIR</b>	2.486	2.473	2.463	2.458	2.454	<b>2.47</b>
<b>CIL+CIR</b>						<b>2.03</b>

Table 4: Results of the experiments with the inclined phantom. LI = leaf spring incline, CIL = control incline left, CIR = control incline right.

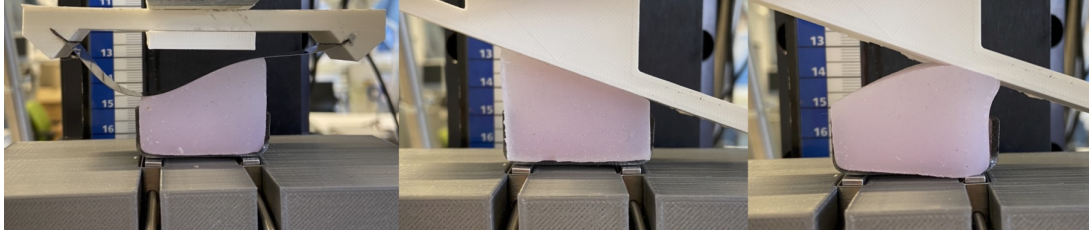


Figure 26: The three combinations the inclined phantom was tested with. From left to right: leaf spring, control (left), control (right).

#### 4.5.3 Leaf spring performance at an angle

Looking at the  $\Delta F$  measured by the load cells, the leaf spring mechanism performs better when not placed at an angle of  $8.5^\circ$ . To compare outcomes: the average  $\Delta F$  of the leaf spring combined with four phantoms with no inclination was 0.62 (table 1 and table 4) versus 1.32 with inclination. This is a difference of 0.70. The altered performance of the leaf spring mechanism can be explained by the fact that, due to the inclined configuration, the phantom does not hit the leaf spring at the center and at right angles with the surface. This causes the deflection of the mechanism to be biased towards one direction. The structure loses its "arch strength".

The top surface pressure-sensitive film results somewhat juxtapose the results obtained from the load cells. Whereas the control films mostly show localised pressure hot spots, the leaf spring films show a more gradual distribution of colour. This is especially the case when looking at the measurements with the inclined phantom. Figure 27 compares them. The control mechanism has no shape-adaptive capabilities so it can only compress what it touches naturally.

The conclusion on superior performance is a matter of perspective. Looking at the differential pressure below the tissue taken at the extremities of the tissue, the control mechanism hence the traditional situation wins. However, film measurement taken from the top surface show localised pressure hot spots similar to the research discussed earlier and shown in figure 40. It is the phantom material deformation that makes up for these inconsistencies as the the forces are guided towards the bottom.

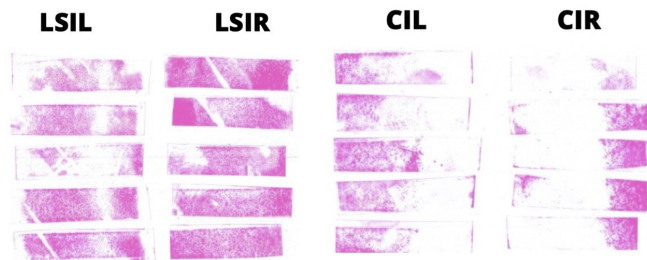


Figure 27: Top-surface pressure-sensitive film results. From left to right: leaf spring/incline (left), leaf spring/incline (right), control/incline (left), control/incline (right).

#### 4.5.4 Conclusion

The pressure-sensitive film measurements show that the pressure distribution on the clamped surface is better in experiments with the leaf spring mechanism than with the control mechanism. The load cell results show that the differential pressure  $\Delta F$  across the bottom surface's extremities is smaller in experiments with the control condition. The leaf spring's performance ( $\Delta F$ ) at an angle is inferior to its performance when flat. However, the four phantom average  $\Delta F$  of the leaf spring at no inclination is still smaller than the four phantom average  $\Delta F$  of the control mechanism at an angle. This means that the leaf spring outperforms the "traditional" situation, but it has to approach the target at an angle as small as possible. This can be corrected for by inclined placement of the mechanism in the upper jaw.

#### 4.5.5 Further considerations

**Shape and size of phantoms** The shape and size of the phantoms used has been iterative process. Initially, the size of the phantoms was fully dependent on the pressure-sensitive film that was used. The film was selected to measure in the lowest possible pressure range, being from 0.006-0.05 MPa. Knowing the amount of force that was going to be exerted onto the phantoms, the contact area of the phantom/film interface could be calculated so that the phantom exerted the right amount of pressure to the film (equation 3). This is why the bottom surface of each phantom is identical.

$$\rho = F/A \quad (3)$$

The top surface area was not the same across the phantoms. Realisation of identical surface areas would overcomplicate the phantom design, as any irregularity on the surface within the set dimensions for  $x$  and  $y$  (the calculated bottom surface area) would mean that the top surface area was larger than the bottom surface area. This would not have been a problem if the flat phantom wasn't used, but this phantom was considered an important condition to test. Another discrepancy between the phantoms was how force was transmitted through the phantom. Looking at figure 22 and 23 and the results that came out of these two experiments, we can conclude that the top shape has a great effect on how volume shifts hence how force is transmitted. Force applied on top could potentially not fully reach the bottom but result in volume shift in different directions. In our clamping situation, forces in different directions would not be accounted for as compression and it would not be relevant to measure them. This is why regulation of applied force or pressure on top of the phantom seemed like an unreliable control variable. The decision was made to regulate the total force measured under the phantom so that there was certainty of the measured force being compression.

**Control mechanism** The control mechanism served to mimic the traditional clamping situation that occurs in most BVS devices, i.e. the scissor clamp (figure 3). This was done by vertical displacement that caused collision between the phantom and an inclined rigid surface. Looking critically, we cannot say that the control condition and the actual situation are identical. Figure 28 illustrates the difference. In the real situation, the clamping action is a rotary movement in which the angle of occlusion between the two jaws declines. In the control condition the angle of occlusion stays constant. Instead, the upper jaw lowers down onto the phantom.

Compare the control condition as if an object is sliding down a slope, but instead of gravity pulling down the object, it is the slope that pushes down onto the object. The friction force is calculated by multiplication of the normal force with the coefficient of friction (equation 5). This normal force is calculated by multiplication of the gravitational force with the cosine of the slope (equation 4). A decline of the slope means that the outcome for the normal force increases. According to the equation, this results in a higher friction force.

$$N = mg\cos(\theta) \quad (4)$$

$$F_{friction} = N\mu \quad (5)$$

From this we can conclude that the friction force increases with a decline in angle, while in the control condition this stays constant. Nonetheless, the difference in nature of the clamping configurations was considered negligible for this type of experiment and data processing, hence the vertical displacement control condition was used.

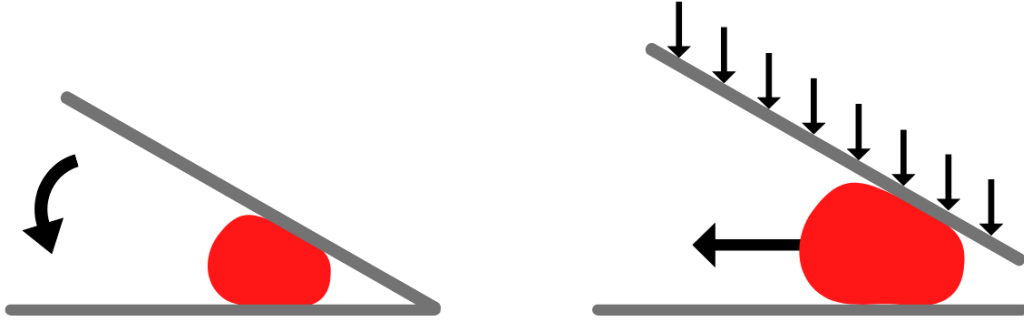


Figure 28: Comparison between the real clamping situation (left) with the control condition (right).

**Phantom support plate** The phantom support plate is a strip of double-bent steel that holds the phantom and the pressure-sensitive film. This plate is connected directly to the load cells with set screws. After several redesigns, the decision was made to give the plate short raised edges. The main incentive to do this was that phantom volume shifted to the sides too much upon compression, affecting results. The raised sides kept the phantom in place and made sure that the exerted force did not get lost in lateral volume displacement. Comparing to the actual BVS clamping situation, this also seems more realistic since tissues also have neighbouring tissues attached to them, restricting their lateral deformation. The only situation in which this does not apply is when a completely separated blood vessel is sealed. Note that this is not a common situation as the blood vessels to be sealed by BVS devices are generally surrounded by connective tissue [24].

The phantom support plate with raised edges did cause an adverse reaction. Too much pressure on one of the sides due to lateral volume shift turned the plate into a lever with the nearest bend as a pivot. This caused the other end to raise slightly, creating a tension force on the load cell. The result was that the load cell measured a negative value of force, something that would not happen in real life. However, the only case in which this occurred was the trapezium/flat combination (figure 24 image 4). As this combination was quickly declared unsuccessful, there was no need for alteration of the support plate.

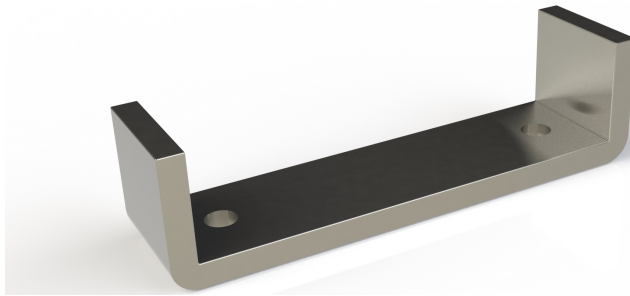


Figure 29: The phantom support plate.



**3D deformation of phantoms** So far, the situation has been treated like a 2D problem, as the problem of nonuniform pressure distribution in BVS devices occurs over the length of the jaws, not the width. However, pressure exerted on the top surface must also result in volume shift in the anterior and posterior direction, especially because movement in this direction is unconstrained (no raised sides). The reason why the pressure distribution along this axis is not monitored is simple; it is symmetrical. All the deflective motion and surface irregularities in the entire mechanism/phantom space occur in the 2D plane the problem was defined in, i.e. the y-plane in  $\mathbb{R}^3$ . This means that the motions and forces occurring in the x-plane always remain constant as long as the y and z values don't change. From this we can conclude that the volume shift in anterior and posterior direction is symmetrical as well, i.e. the same for each side. Monitoring this would not make sense because two load cells positioned opposite each other in the x-plane would always measure the same value.

**Orientation of phantoms** The peak and incline phantom are not symmetrical along the y-plane. This means that a change in the orientation of the phantom in the y-direction would affect the motion of the mechanism hence individually measured values of the load cells. Nonetheless,  $180^\circ$  rotation of the phantom would still deliver the same value for  $\Delta F$ . This is due to the symmetrical nature of the mechanisms and the fact that phantoms were always placed under the center of the mechanisms. Rotation of the phantom would cause the same mechanism deflection and the same individual load cell values, but mirrored. By taking the absolute value of the difference between the two, this asymmetry in the peak and incline phantom is overcome (equation 2). The only mechanism that is not symmetrical is the control condition. The preceding explanation does not hold for this situation. To overcome this discrepancy, the experiments were performed twice when the control mechanism was tested with an asymmetrical phantom. The five measurements were performed for both phantom orientations and the average was taken as the final result.

**Amount of force exerted** The amount of force exerted on the phantoms was not inspired by actual vessel sealing forces, as far as these ideal values exist. Chekan et al. (2014) have shown that the pressure exerted on tissues varies greatly between BVS devices. To give an example: the ENSEAL Articulating device exerts almost 5 times the distal tip compression as the LigaSure device [25]. This discrepancy called for research. Lether (2020) wrote a literature survey on the ideal clamping compression for bipolar vessel sealing. He compared different pressures with the burst pressure (BP) of the sealed vessel. The conclusion was that the best seal is achieved with a compression of  $800 \text{ mN/mm}^2$  [3]. Looking at our phantom bottom surface area of  $360 \text{ mm}^2$  and using equation 3, this would come down to 288 N. This force is too high for adequate testing within our experiment space. The mechanisms would need upscaling in size and strength. To reach the average pressure value the FujiFilm 5LW film measures in, the phantom bottom surface area would need to be  $10000 \text{ mm}^2$ , e.g.  $100 \times 1 \text{ cm}$ . Another reason why this "ideal" pressure was not used in the experiment is the question whether this value is scalable. The literature survey by Lether is about actual BVS devices with a diameter of 5 mm. The mechanisms and phantoms used for this experiment have dimensions of roughly 10 times that value. The compliant mechanism deflection and the phantom deformation are nonlinear in nature, so conversion of ideal pressures would overcomplicate the experiment. The final  $7 \pm 0.1 \text{ N}$  was chosen because it showed desirable deflection and deformation in the mechanisms and phantoms respectively. This value also allowed the system to exert the right amount of pressure for the pressure-sensitive film to function.

## 5 Embodiment design

This section describes how the choices made throughout the process come together in a practical model of the redesigned bipolar vessel sealer. This comprises the more prevailing parts, such as the hinge or the distribution mechanism, as well as smaller components that need argumentation for their incorporation.

The final model of the redesigned bipolar vessel sealer was inspired by the Steerable and Reusable Bipolar Vessel Sealer designed by Philip de Haes [26]. His design can be seen in figure 51 in the appendix. Apart from the general design language, some functional parts that Philip used have been incorporated into this design, simply because they enhance the product. These parts will be handled later in this section.

### 5.1 Design choices

#### 5.1.1 Distribution mechanism

The distribution mechanism that performed the best during the experiment was the leaf spring. Incorporation of a mechanism that tiny into a laparoscopic device with a 5 mm diameter is complicated, but the crux was the fact that everything should be cleanable. The decision had quickly been made that the mechanism was going to be a magnetic insert in the upper jaw. This insert is the only disposable part in the entire product. Making the insert disposable was also fueled by the concern that the articulating steel sheet might be subject to fatigue, wear and plastic deformation. If the steel is dented or folded during use, e.g. by accidental clamping of rigid structures or other equipment, the mechanism could lose all of its pressure distributing properties or even create pressure hot spots on the sites of damage.

The magnetic insert can be seen in figure 30 and 31. The mechanism has been embedded into the insert, only partly protruding from the bottom. A notch has been made so that the mechanism has full space for deflection and shape adaptation. The reason why the steel sheets are embedded is that the mechanism could otherwise block full occlusion of the jaws. Having the sheets protrude from the bottom surface without any underlying notch also facilitates plastic deformation of the sheets when the jaws are fully occluded. The notch serves as a buffer and protects the steel sheets.

The additional experiment granted the insight that the leaf spring mechanism shows inferior performance when placed at an angle. To compensate for the naturally inclined configuration of the upper jaw, the leaf spring insert has been designed so that it counteracts this angle. This is done by placing the mechanism at the same  $8.5^\circ$ , but mirrored. The principle has been illustrated in figure 30.



Figure 30: Inclined configuration of the leaf spring mechanism.

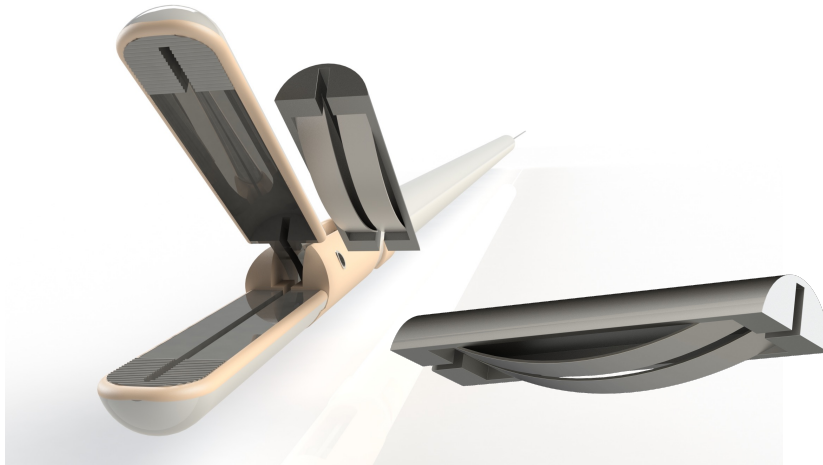


Figure 31: The magnetic insert with the distribution mechanism, to be placed in the cavity in the upper jaw.

### 5.1.2 Hinge

The choice was made to use the "blade slit" as the hinge during the conceptualisation phase. This mechanism allows for one-step actuation of the jaw and blade by having an attachment of the upper jaw slide through a cutout profile in the blade. For the incorporation of this system, the casing for Philip de Haes' SATA hinge was altered to fit the blade slit hinge. The mechanism and its functioning can be seen in figure 32. During the conceptualisation phase, the mechanical feasibility of the blade slit system was examined by drawing a free body diagram (figure 32) and balancing the equations in Excel. This model allowed for tweaking of dimensions to come to desirable values.

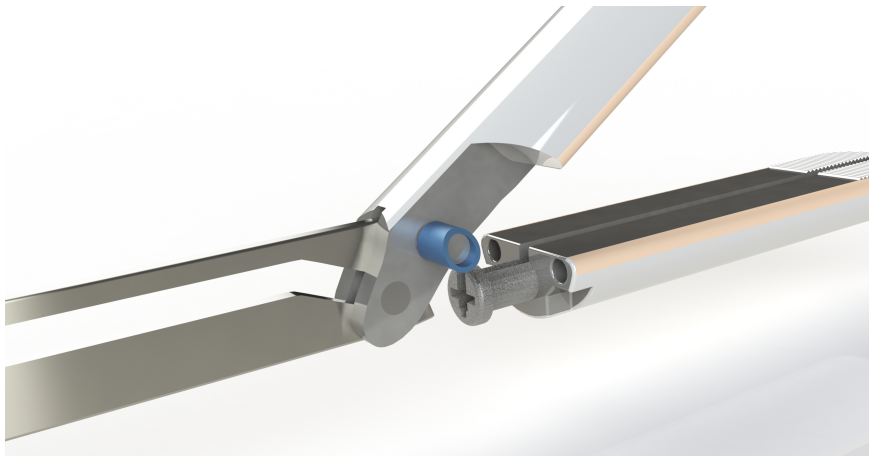


Figure 32: The blade slit mechanism for one-step actuation of jaw and blade. Note that the blue axes are fixed to the casing, which is left out in this image for distinctness. To visualise the working principle of the mechanism, one should imagine the blade (left) to move towards the jaws through the slit. The axis which is attached to the upper jaw is guided upward through the cutout profile in the blade. This upward motion of the axis causes the upper jaw to move downward.

### 5.1.3 Connection shaft/hinge

The shaft can be connected directly to the lower jaw by the use of two conductor rods. These rods supply the jaws with current for tissue sealing and keep the paths of current flow separated. The ends of these rods have insulating buttons on them that click into holes in the shaft. This secures the shaft to the tip. By pushing the buttons inward, the shaft is disconnected and can be taken off for sterilisation. The system can be seen in figure 33.

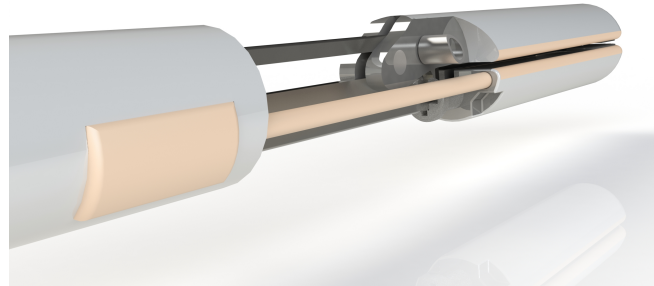


Figure 33: A rendering showing the click mechanism used to secure the tip to the shaft.

### 5.1.4 Partition of current flow

It is important that the electrodes and the jaws are separated from each other with an insulating layer. The only location at which current is allowed to pass is the sealing surfaces. Philip de Haes performed research on the possibilities of having the current flow through the product parts themselves instead of using separate electrodes. Incorporation of this would boost cleanability tremendously as there are no pieces of electronics in the shaft that need to be taken out. The idea of Philip was adopted and incorporated. Figure 34 shows working principle. The red parts are the active electrode and the blue parts the return electrode. When the sealing mode is activated, current flows from the blade into the upper jaw to the distribution mechanism and the serrated teeth at the very tip. Current passes through the tissue to the lower jaw. The lower jaw guides the current through the conductor rods to a conducting inner lining of the shaft. Insulating coatings have been applied to every conducting part except for the sealing surfaces so that current flow paths do not intertwine. The jaws have been encapsulated by steel casings that have an inner lining of insulating coating. Between the shaft and the tip rests a connective part that holds the axis of the upper jaw. This part will be made of PEEK, an polymer with excellent insulating properties.

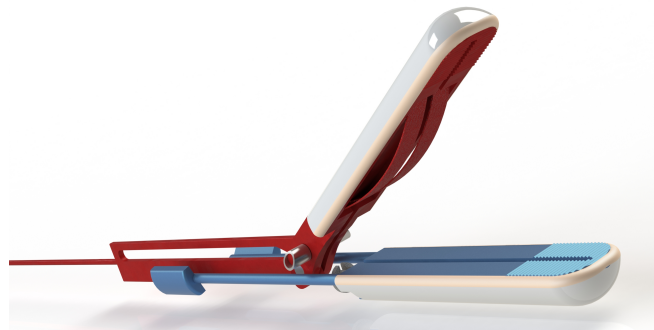


Figure 34: Partition of current flow in conducting product parts. The red parts form the active electrode and the blue parts the return electrode.

### 5.1.5 Blade

Many manufacturers use completely different types of blade and little have proper argumentation to support this. Figure 41 in the appendix shows a selection of some of the blade shapes that have been encountered. After sifting through manufacturers' websites and patents, the conclusion has been drawn that this variation in blade shapes is most probably due to a patent-related rationale. However, one manufacturer that is more explicit about their choice of blade is KLS Martin, the owner of the reusable MarSeal5 plus bipolar vessel sealer. This device uses a concave blade geometry to ensure that the tissue is automatically guided towards the center of the blade. The company claims that chamfered blades lead to tissue slippage and tissue not being severed [27]. Two comparative illustrations can be seen in figure 35.

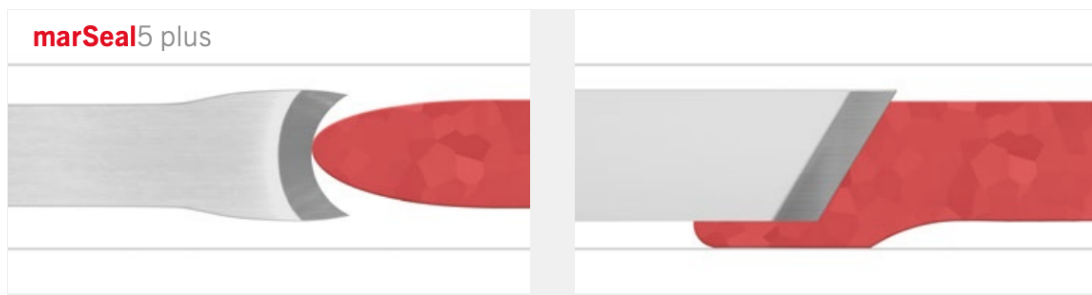


Figure 35: A concave blade (left) and a chamfered blade (right). Chamfered blades could cause tissue slippage and tissue not being severed [27].

Prevention of tissue slippage adds to the functioning of the design. This is why the idea of a concave blade was adopted. The final design with the cutout profile for upper jaw occlusion can be seen in figure 36.

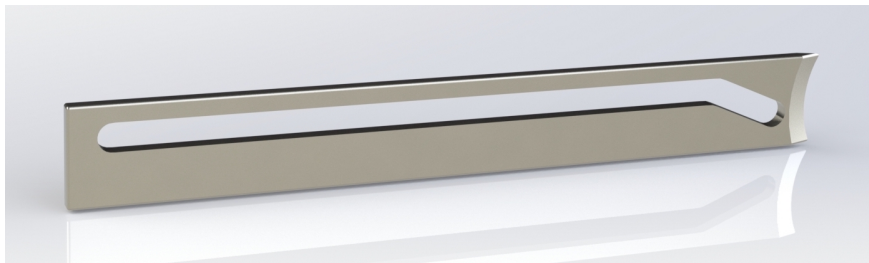


Figure 36: The concave blade with the cutout profile for upper jaw occlusion.

### 5.1.6 Jaws

There is huge variety of shapes and sizes on the bipolar vessel sealing market when it comes to designing the jaws. It is common for brands to launch two versions of each product: one with straight jaws and one "Maryland" edition with curved jaws. Despite the advantages of curved jaws being proposed by the market, the decision has been made that the redesigned BVS device will have straight jaws. A curved jaw would overcomplicate the design of a distribution mechanism, which was known to become an insert. Application of a Maryland jaw would be interesting for further development of the product.

If we were to call the variation between straight jaws and Maryland jaws to happen in the transverse plane of the tip, there is also a choice to be made in the sagittal plane. A snippet of the variation that exists between current BVS devices is illustrated in figure 52. When considering this, the conclusion was drawn that it would be wisest to go for a shape that maximises the volume used inside the 5 mm diameter, given that this scarce space is going to contain

several elements including the distribution mechanism insert. The shapes that correspond to this desire are the ones of LigaSure Covidien and Lamidey Noury Thermocut.

The final aspect to take into consideration was whether to apply a grip pattern to the jaw to prevent tissue slippage. The initial thought was that incorporation of an irregular surface would negatively influence the uniformity of the pressure distribution. However, Richter (2006) et al. have shown that "structured" surfaces have a lower seal failure rate than "smooth" surfaces [28]. To get a more hands-on opinion on this, surgeon Roelf Postema was contacted through email. He replied that he has no experience with serrated jaw surfaces, but he did see the relevance of using them in the design because of improved tissue fixation between the jaws (figure 42). With this insight, the conclusion has been drawn to incorporate a grip surface at the end of the tip, to be seen in figure 37.

The jaws were designed to use as much of the volume as possible within the 5 mm diameter range. A serrated grip pattern has been added to the tip for enhanced grip during manipulating of tissues. The design can be seen in figure 37.

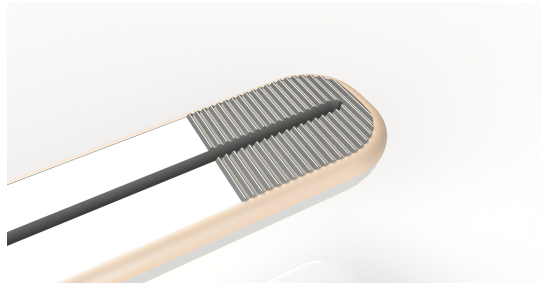


Figure 37: The lower jaw with a serrated surface for grip.

### 5.1.7 Coating for friction

Apart from the serrated teeth at the very tip, the articulating surface of the steel sheets should also be able to generate enough friction to keep the tissue in place when clamped. Without this, tissue could slip away and miss out on the distributing properties of the mechanism. The decision was made to enrich the steel sheets with a tungsten carbide coating. Tungsten carbide is a material used in surgical equipment due to its wear-resistant and frictional properties. Depending on the coarseness of the grits applied, the holding force of a clamp can increase by a factor 3 [29].

### 5.1.8 Choice of material

The material used throughout the product is surgical steel, i.e. austenitic SAE 316. Due to its resistance to corrosion and good strength it is the best material to be working with. The paths of current flow are separated by a dielectric coating. This can be made with a variety of oxide ceramics such as oxides of aluminum, titanium and yttrium [29].

## 5.2 Technical design

Several analytical models have been made to predict the behaviour of different parts of the device. For the distribution mechanisms, the models served as a medium to calculate the dimensions necessary to achieve the desired amount of deflection. The models for the spring toy and trapezium mechanism can be found in the appendix. No model of the leaf spring mechanism could be made due to the high level of nonlinearity. The steel sheet thickness was determined by trial and error instead.

Another model was made to calculate the push force  $F_{push}$  that the blade has to exert to occlude the upper jaw. The model has been illustrated in figure 45. It calculates the push force with the clamp's dimensions, the required clamping force  $F_n$  and the opening angle of the jaw  $\beta$ . Using equation 3, the ideal clamping force could be calculated using the ideal pressure found by Lether [3] and the clamping surface area of the jaw. This ideal force turned out to be 65.5 N. By inputting this force into the model, an ideal  $F_{push}$  was calculated to be 330.7 N (figure 5) in the appendix) upon full occlusion. We can conclude that this is a lot of force to produce by hand with the trigger on the handle. This topic is further elaborated on in the discussion.

The last point of concern was the downward force  $F_{p,y}$  that the upper jaw axis exerts on the blade when when closing. According to the model and figure 5, this force is 798.4 N when fully occluded. This is a large force to exert to a 0.5 mm thick steel sheet. The finite element method (FEM) was used to analyse the situation and it gave positive results. The maximum strain under the upper jaw axis was 0.013 mm. This means that no severe damage is done to the blade. The full FEM report can be found in the appendix.

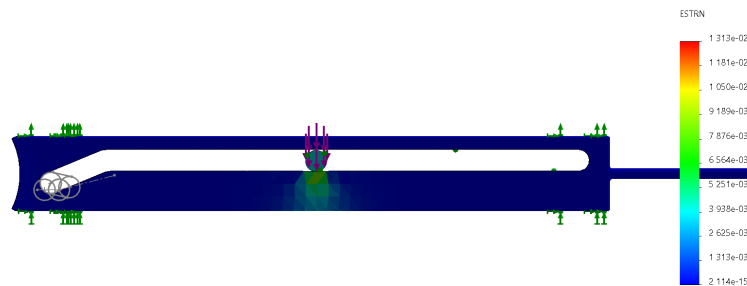


Figure 38: The FEM report showing the strain in the blade and axis when the "ideal" force is exerted by the upper jaw at full occlusion.

### 5.2.1 Free Body Diagram verification

The most important concern was the forces that this type of actuation would exert on the jaw closing system. The design will consist of small and thin parts, so one should be cautious of unwanted deformations. The forces were balanced in a Free Body Diagram that can be seen in figure 45 in the appendix. The equations were entered into an Excel model so that the dimensions could quickly be tweaked to reach the desired values.

### 5.2.2 Rapid prototyping

A test prototype of the new "blade slit" closing mechanism was made to verify the working principle of this system. This was done using a simple FDM printer with PLA as the filament. The quick manual test worked out successfully and showed that the blade slit idea could become functional in the eventual design, given that the dimensions allowed the right forces to be exerted. The prototype can be seen in opened and closed position in figure 39.



Figure 39: The prototype of the "blade slit" occlusion mechanism. In this configuration, the blade is positioned halfway.

## 6 Discussion

After a period of extensive ideation, conceptualisation and validation, a reusable and pressure distributing BVS device was created. This last section will be used to reflect on the redesigned product and its functionalities. The thesis started with a design goal and a list of design requirements. Together they will serve as criteria to test the success of the design. The section will end with a series of future recommendations for further development of the design.

### 6.1 Design goal

The design goal was constructed at the very beginning of the process.

**“Design a state-of-the-art reusable bipolar vessel sealer that can be cleaned along with other surgical equipment due to a modular architecture and that applies a more uniformly distributed pressure to the tissue, improving its performance and making it suitable for use in LMICs.”**

To structure the scoring of the redesign’s adherence to the design goal, the phrase has been deconstructed to its essential parts.

**”reusable/that can be cleaned along with other surgical equipment”** As stated before, the term ”reusable” is a concept that is hard to prove within current resources. However, several great innovations have been incorporated into the tip that promote cleanability. In a traditional BVS device, the shaft is filled with products parts such as the blade actuator, the jaw actuator and the active and return electrode. In this redesign, all the parts have been reduced to one single part: the blade. This dramatic reduction means that the shaft will be empty upon removal of the blade when disassembled. When positioned properly, modern-day autoclaves are capable of proper sterilisation of lumen this thin and long [30]. Next to that, other measures have been taken to improve cleanability, like rounded edges and as little small spaces as possible. The really small spaces like the blade slit in the upper and lower jaw could need extra care with a cleaning tool, but research would have to prove that. The PEEK base has been designed for accessibility; the top and bottom are open so that the autoclave can reach the parts inside.

**”due to a modular architecture”** The device is built to be modular as it needs to be taken apart as much as possible for cleaning and sterilisation. The shaft can be released with the click mechanism. This leaves the user with the upper jaw, lower jaw, PEEK base, blade and distribution mechanism insert. The insert can be taken out with force. Without special equipment, this is what goes into the autoclave. Consider the shaft, the blade, the insert and jaws/PEEK base combination as four parts that are modular and can be replaced by the hospital staff themselves.

**”applies a more uniformly distributed pressure to the tissue”** The incorporation of the leaf spring mechanism makes the newly designed BVS device distribute pressure more uniformly than the control mechanism used in the experiments. This control mechanism was constructed to mimic the conventional BVS clamping configuration. Taking the average performance of the four phantoms used at no inclination, the difference in  $\Delta F$  between the leaf spring mechanism and the control mechanism is 0.16 N.

**”making it suitable for use in LMICs”** The ideal of ”suitability for use in LMICs” is a characteristic that is hard to quantify. However, we can refer back to the problem definition in the beginning of this thesis. ”Laparoscopic devices are generally more expensive, have more complex sterilisation procedures and require special training.” It is the second hurdle that forms the incentive for manufacturers to label their devices as disposable. Doing this saves



them time and money as no measures have to be taken for cleanability. The current situation is that LMIC hospitals cannot afford the disposal of BVS devices, leading to unrightful reuse (up to 30/40 times). Since risk of nosocomial infection does not seem to be a big concern in LMIC hospitals, the newly designed BVS device needs to pose a legitimate advantage, most probably expressed in terms of costs. This means that the average price per use cycle must be lower than the price of using a disposable device for 30/40 times. Regardless of the purchase prices of either the disposable or reusable device, this objective can always be achieved by making the reusable device durable [31]. The redesigned BVS device that came out of this research was designed to be durable and modular. LMIC hospitals will have to consider it an investment, but purchase of this device will benefit them financially over time.

## 6.2 Design requirements

The second chapter on background information ended with an extensive list of design requirements. This list has been copied below. Check marks have been applied to the requirements that were successfully met.

### The device should...

1. be able to seal blood vessels. ✓
  - (a) prevent leakage of electricity by the use of insulating coatings. ✓
  - (b) seal blood vessels up to 7 mm. ✓
  - (c) grasp and manipulate tissue. ✓
  - (d) be able to divide the tissue with a blade. ✓
  - (e) have straight jaws. ✓
2. be cleanable and sterilisable. ✓
  - (a) be modular. ✓
    - i. not rely on electrical wires for transport of energy to the tip. ✓
    - ii. allow disassembly. ✓
      - A. have a low number of modular parts. ✓
      - B. have clear use cues on how to disassemble. ✓
      - C. have a maximum of two moving parts per clamping jaw. ✓
    - iii. allow access throughout the entire shaft (open lumen for cleaning). ✓
    - iv. have a fully removable blade. ✗
  - (b) have a mechanism made of surgical steel. ✓
  - (c) rely on a compliant mechanism. ✓
  - (d) distribute the pressure on just one jaw. ✓
  - (e) have a more cleanable hinge than conventional BVS devices. ✓
3. be reusable. ✓
  - (a) perform jaw occlusion and tissue dissection with just one actuation.
  - (b) withstand forces that are exerted on the device by surgical use and cleaning. ✓
  - (c) allow for replacement of modular parts. ✓
4. exert a uniformly distributed pressure of 800 mN/mm<sup>2</sup> to the tissue throughout the entire clamping process. ?
  - (a) allow for adaptation to surface irregularities of +/- 0.5 mm. ✓
  - (b) allow for mechanism distortions up to 6 degrees. ✓

- (c) use a shape-adaptive approach to clamp the tissue. ✓
- 5. adhere to the dimensions for laparoscopic instruments. ✓
  - (a) have an outer diameter of 5 mm. ✓
  - (b) have a shaft + tip length of more than 33 cm. ✓
  - (c) have a seal length of 20 mm. ✓
- 6. be safe. ✓
  - (a) not contain any sharp edges that could damage the surroundings. ✓
  - (b) be constructed of biocompatible materials. ✓

Almost all requirements have been met successfully except for requirements 2(a)iv and 4. Requirement 2(a)iv is about the blade being fully removable. This is a useful step that promotes cleanability. However, the current jaw occlusion mechanism with the blade slit hindered this ideal. The idea was to have the cutout profile extend all the way to through the back of the blade. This is where the upper jaw axis could enter and leave the blade profile. The reason why this was stamped unfeasible is because of the high forces that are exerted onto the system. Leaving the back of the blade open would severely weaken the structure. Next to that, the final configuration of the product would not allow the blade to exit the device through its back opening. There is no space to extend the blade forward enough for the upper jaw axis to reach the opening. The solution would be that the blade is extended diagonally, either up or down, through the openings in the PEEK base. This would require a slit to be cut out of the base, weakening the structure that holds the upper jaw axes.

Requirement 4 is about the device exerting the ideal sealing pressure found by Lether [3]. The question mark has been inserted at the end of the line because the solution for this problem does not lie inside the shaft/tip design space, which this thesis limits itself to. In the current configuration, a relatively high pushing force is needed for the blade to occlude the upper jaw. This high force must be generated inside the handle. This could be done using lever systems or use of an electrically actuated blade.

## 6.3 Recommendations

There there are some aspects of the product that would benefit from further research and development. This section will handle the possible shortcomings and opportunities of the design.

### 6.3.1 Circuitry

The device uses the conductive properties of its own product parts to transport energy from the handle to the tip and back. Successful incorporation of this principle would require research on the effect of the different conducting parts to the radio frequency current. The current in bipolar vessel sealing is traditionally controlled through an active feedback loop, measuring the current that returns and altering the active current real-time. This prevents unintended tissue damage or inadequately sealed vessels. Further research would need to justify the feasibility of this principle through self-conducting parts.

### 6.3.2 Low thickness

Due to the limited amount of space inside a 5 mm diameter device, some parts ended up having a low material thickness. This could affect the mechanical functioning of the device, potentially leading to deformation or wear. More research could be done to find space-saving solutions, allowing thicknesses to be higher.

### **6.3.3 High pushing force**

The current configuration of the jaw occlusion mechanism requires the blade to be pushed forward with a relatively high force in order for the upper jaw to be able to exert the "ideal" sealing pressure. Further research and a redesign with different dimensions could solve this problem. There was not enough space in this design for levers long enough to relieve the force required to achieve the desired moment in the rotational axis of the upper jaw. This problem could potentially be solved by a lever that extends from the device (outside the 5 mm) whenever the device has reached its destination, hence has passed the 5 mm trocar.

### **6.3.4 Scalability**

The experiment that tested the pressure distributing capabilities of the three distribution mechanisms was conducted at a scale about 10 times as large as the real-life situation. Due to the high level of nonlinearity in the leaf spring mechanism, certainty of similar functioning at a smaller scale lacks. The problem would be solved by conducting the experiment at the 5 mm scale and using authentic forces, but this requires professional fabrication of parts, state-of-the-art sensors and highly precise actuators.

### **6.3.5 Cleanable distribution mechanism**

The distribution mechanism is the only disposable item in the redesign. This is due to small cavities that hinder cleanability, as well as the nature of the leaf spring mechanism itself. Because the compliant part is the articulating surface itself (instead of a rigid part like in the other mechanisms), plastic deformation would mean that the next tissue will be clamped by a "folded" surface. This can create pressure hot spots and would completely rid the mechanisms of its distributing capacities. Research to eliminate the chance of plastic deformation in the steel sheet is necessary, next to a redesign of the insert to promote cleanability.

### **6.3.6 Cleaning tool**

Handheld cleaning tools that are designed to clear cavities and narrow spaces could be added to the product packaging. Execution of a few simple cleaning steps before full sterilisation could enhance cleanability even further. This idea was inspired by the marSeal5 plus by KLS Martin. Their product comes with a special cleaning tool and a rinsing adapter set for the shaft.

### **6.3.7 Blade removal**

Being able to remove the blade would be a huge step in the direction of cleanability and modularity. The blade is a part that is subject to wear and the product would benefit from facile replacement thereof. A redesign of the product is necessary to allow for blade removal. An alternative to having the upper jaw axis "escape" the blade slit profile could be to remove the upper jaw axis from the upper jaw. In the current configuration, this axis is simply too small for the hospital staff to do this and a minuscule mechanism would need to be designed to secure the axis in place.

### **6.3.8 Haptic feedback**

It would be wise to add a haptic feedback system to the product so that the surgeon knows when the jaw closing phase switches to the tissue dissection phase. This is not present in the current design, potentially leading to accidental tissue damage when the device is used as a regular pair of forceps. The solution could be either haptic, so the surgeon can feel the transition, or it could be a mechanism that prevents the blade from entering the sealing area unless a certain action is undertaken (e.g. pressing a button).

### **6.3.9 Insert fixation**

The distribution mechanism insert is meant to be held in place by magnetism. This eliminates the need for construction of a minuscule fixation system. For proper incorporation of this concept, more research is needed to validate the functioning of magnetic fixation in a BVS device.

## **6.4 Conclusion**

A redesigned bipolar vessel sealing device has been constructed with the goals of improving reusability and pressure distribution. The decisions made for the redesign have been fueled by analysis, conceptualisation and experimental validation. At the beginning of the project, a design goal and a set of design requirements have been formulated. The goal has successfully been met. All requirements except for one have been met.

The device has been enriched with a leaf spring mechanism for pressure distribution and a blade slit mechanism for reusability. Next to that, self-conducting parts form the circuit so no separate electrodes are needed. Further research and development is needed for optimal reusability.

## References

- [1] Motta LS Cuschieri A Reyes DAG Brown SI, Cochrane L. Thermal fusion: effects and interactions of temperature, compression, and duration variable. *Surgical Endoscopy*, 26:3626–3633, December 2012. <https://doi.org/10.1007/s00464-012-2386-1>.
- [2] Clymer JW Amaral JF Voegelé AC Korvick DL, Gutierrez M. Perpendicular blood vessel seals are stronger than those made at an angle. *Journal of Laparoendoscopic and Advanced Surgical Techniques*, 23(8):669–672, July 2013. <https://doi.org/10.1089/lap.2013.0028>.
- [3] Lether R. Bipolar electrosurgical graspers. *Faculty of Mechanical, Maritime and Materials Engineering (3mE)*, Delft University of Technology, April 2020.
- [4] Garry R. Laparoscopic surgery. *Best Practice Research Clinical Obstetrics and Gynaecology*, 20(1):89–104, February 2006. <https://doi.org/10.1016/j.bpobgyn.2005.10.003>.
- [5] Obstetrics Selva’s Fertility and Gynaecology Clinic. <https://www.melakafertility.com/laparoscopic-surgery/>.
- [6] Hanisch E. Buia A, Stockhausen F. Laparoscopic surgery: A qualified systematic review. *World Journal of Methodology*, 5(4):238–254, December 2015. <https://doi.org/10.5662/wjm.v5.i4.238>.
- [7] Gnanaraj J Brown J Jayne D. Wilkinson E, Aruparayil N. Barriers to training in laparoscopic surgery in low- and middle-income countries: A systematic review. *Tropical Doctor*, 51(3):408–414, April 2021. <https://doi.org/10.1177/0049475521998186>.
- [8] Opoku-Anane J Maine R Chao ET, Mandigo M. Systematic review of laparoscopic surgery in low- and middle-income countries: benefits, challenges, and strategies. *Surgical Endoscopy*, 30(1):1–10, April 2015. <https://doi.org/10.1007/s00464-015-4201-2>.
- [9] MacCormick AD Siu J, Hill AG. Systematic review of reusable versus disposable laparoscopic instruments: costs and safety. *ANZ Journal of Surgery*, 87(1-2):28–33, February 2017. <https://doi.org/10.1111/ans.13856>.
- [10] Wauben LSGM Madete J Groen RS Oosting RM, Dankelman J. Roadmap for design of surgical equipment for safe surgery worldwide. *Proceedings IEEE Global Humanitarian Technology Conference (GHTC 2018)*, pages 1–8, January 2019. <https://doi.org/10.1109/GHTC.2018.8601913>.
- [11] Duprè G Gardeweg S, Bockstahler B. Effect of multiple use and sterilization on sealing performance of bipolar vessel sealing devices. *PLoS ONE*, 14(8), August 2019. <https://doi.org/10.1371/journal.pone.0221488>.
- [12] Naylor C McGain F. Environmental sustainability in hospitals - a systematic review and research agenda. *Journal of Health Services Research and Policy*, 19(4):245–252, May 2014. <https://doi.org/10.1177/1355819614534836>.
- [13] Balkenende R Kane G, Bakker C. Towards design strategies for circular medical products. *Resources, Conservation and Recycling*, 135:38–47, August 2018. <https://doi.org/10.1016/j.resconrec.2017.07.030>.
- [14] Georgescu C. Report of the special rapporteur on the adverse effects of the movement and dumping of toxic and dangerous products and wastes on the enjoyment of human rights. *Human Rights Council*, September 2011. <https://doi.org/>.
- [15] Hoogeweegen A. Detachable steerable clip applicator for dissection of its branches. *Delft University of Technology*, October 2017. <http://resolver.tudelft.nl/uid:c530fe51-e578-4466-a848-01bd33d2afb8>.

- [16] Cross JA. Mechanisms to achieve a uniformly distributed pressure across a clamped surface. *Faculty of Mechanical, Maritime and Materials Engineering (3mE)*, Delft University of Technology, January 2021.
- [17] Naish MD Patel RV Malthaner RA Kurowski TP, Trejos AL. Design of a minimally invasive lung tumor localization device. *Proceedings of the ASME 2012 5th Annual Dynamic Systems and Control Conference joint with the JSME 2012 11th Motion and Vibration Conference*, 3:411–418, October 2012. <https://doi.org/10.1115/DSCC2012-MOVIC2012-8643>.
- [18] Mehmanesh H Najarian S Farkoush SH, Abolfathi N. Design and finite element analysis of a novel smart clasper for aortic cross-clamping in minimally invasive surgery. *Minimally Invasive Therapy Allied Technologies*, 25(1):15–21, December 2016. <https://doi.org/10.3109/13645706.2015.1054838>.
- [19] Cuschieri A Frank T, Willetts GJ. Detachable clamps for minimal access surgery. *Proceedings of the Institution of Mechanical Engineers, Part H: Journal of Engineering in Medicine*, 209(2):117–120, June 1995. <https://doi.org/>.
- [20] Klar M et al. Comparison of a reusable with a disposable vessel-sealing device in a sheep model: efficacy and costs. *Fertility and Sterility*, 95(2):795–798, February 2011. <https://doi.org/10.1016/j.fertnstert.2010.09.014>.
- [21] Department of Mechanical Engineering. Compliant mechanisms explained. *Brigham Young University*. <https://www.compliantmechanisms.byu.edu/about-compliant-mechanisms>.
- [22] Bibi S et al. Sealing of vessels larger than 7 millimeters using Enseal in porcine aorta. *Journal of The Society of Laparoscopic Robotic Surgeons*, 18(3), July 2014. <https://doi.org/10.4293/JLSL.2014.00182>.
- [23] Rothstein B. What is the difference between surgical steel and stainless steel? *Mead Metals Inc.*, May 2019. <https://www.meadmetals.com/blog/surgical-steel-vs-stainless-steel>.
- [24] National Cancer Institute. Classification structure of blood vessels. <https://training.seer.cancer.gov/anatomy/cardiovascular/blood/classification.html>.
- [25] Singleton DW Mennone JZ Hinoul P Chekan EG, Davison MA. Consistency and sealing of advanced bipolar tissue sealers. *Medical Devices (Auckland)*, 20:8:93–99, April 2015. <https://doi.org/10.2147/MDER.S79642>.
- [26] De Haes P. Steerable and reusable bipolar vessel sealer. *Biomedical Engineering — Medical Instruments and Medical Safety (MIMS)*, November 2020. <http://resolver.tudelft.nl/uuid:0c794bd3-1df5-4904-8121-36055845b8be>.
- [27] KLS Martin. marseal5 plus. [https://www.klsmartin.com/fileadmin/user\\_upload/Homepage/Mediathek/90-334-02\\_marSeal5\\_plus.pdf](https://www.klsmartin.com/fileadmin/user_upload/Homepage/Mediathek/90-334-02_marSeal5_plus.pdf).
- [28] Schilling MK Pistorius GA Menger MD Richter S, Kollmar O. Efficacy and quality of vessel sealing: comparison of a reusable with a disposable device and effects of clamp surface geometry and structure. *Surgical Endoscopy*, 20(6):890–894, June 2006. <https://doi.org/10.1007/s00464-005-0380-6>.
- [29] MITEE-BITE PRODUCTS. Tungsten carbide coating. <https://www.miteebite.com/products/tungsten-carbide-coating/>.
- [30] Chaunet M Dufresne S, Leblond H. Relationship between lumen diameter and length sterilized in the 125l ozone sterilizer. *American Journal of Infection Control*, 36(4):291–7, May 2008. <https://doi.org/10.1016/j.ajic.2007.06.006>.

- [31] Kawaguchi K et al. Reusable vessel sealing device can significantly reduce medical costs compared to disposable device in modified total neck dissection. *Journal of Surgical Oncology*, 3(4):2–4, July 2020. <https://doi.org/>.
- [32] Walberg E Wentz MN Eick S, Loudermilk B. Rationale, bench testing and in vivo evaluation of a novel 5 mm laparoscopic vessel sealing device with homogeneous pressure distribution in long instrument jaws. *Annals of Surgical Innovation and Research*, 7(1):15, December 2013. <https://doi.org/10.1186/1750-1164-7-15>.

## A Appendix

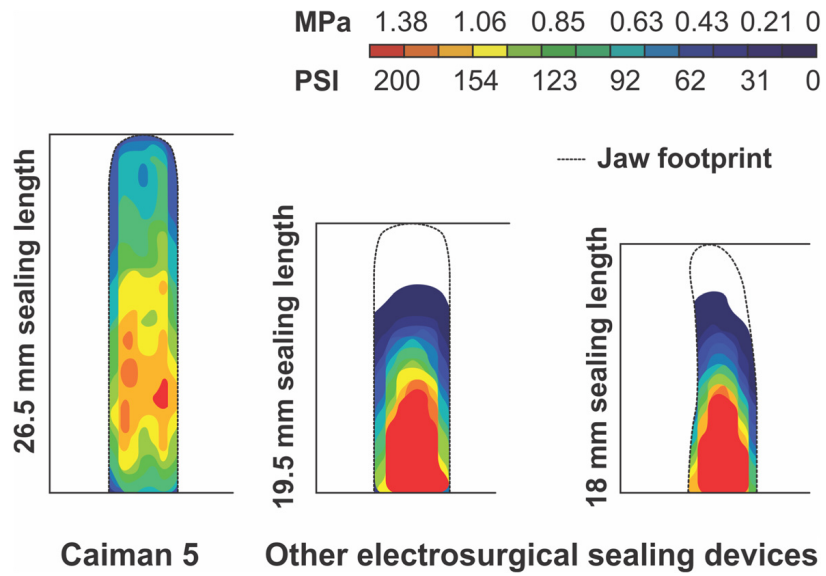


Figure 40: Pressure profiles of B. Braun's Caiman 5 (left) compared to two versions of Medtronic's LigaSure (right). Whereas the Caiman 5 has a relatively constant pressure covering the entire articulating surface of the jaw, the LigaSure devices concentrate pressure near the hinge and exert virtually no pressure near the tip [32].

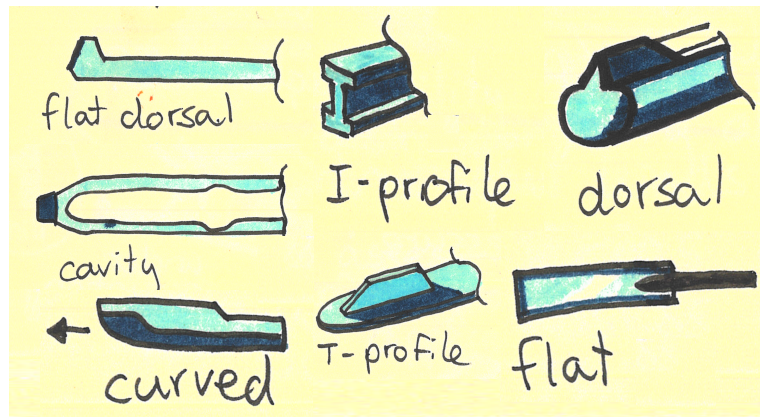


Figure 41: Different shapes of blade used in bipolar vessel sealing.





James Cross &lt;jamesdrucross@gmail.com&gt;

**Vragen omtrent Bipolar Vessel Sealing**

3 berichten

**James Cross** <jamesdrucross@gmail.com>  
Aan: rpostema@spijkennisemc.nl

17 augustus 2021 om 13:12

Beste dokter Postema,

Mijn naam is James Cross en ik ben aan het afstuderen bij Daniel Robertson met bipolar vessel sealers als onderwerp. Hij heeft me uw contactgegevens gegeven opdat ik u een paar vragen zou kunnen stellen hierover.

Welk type weefsel sealt u het meest tijdens operaties? Met andere woorden; als ik een fantoomweesel wil ontwikkelen voor experimenten met vessel sealers, van welk type weefsel kan ik het beste de materiële eigenschappen overnemen?

Sommige vessel sealing devices hebben een tandjesprofiel in de binnenkant van de klem zitten voor grip op weefsel. Andere devices (zoals Caiman 5 en Enseal) hebben dit niet. Vindt u deze gripprofielen nodig voor het grijpen van weefsel of zou dit weggelaten kunnen worden?

Alvast bedankt,  
James Cross**Postema, R (Roelf)** <rpostema@spijkennisemc.nl>  
Aan: James Cross <jamesdrucross@gmail.com>

31 augustus 2021 om 14:51

Hallo James,

Meestal sealen we idd de vaten van bv het mesenterium van de darm of de vaten naar de milt of de maag. Is dus een combinatie van vetweefsel/peritoneum/arterie/vene. Ook in de lever kun je sealen waarbij je probeert zoveel mogelijk de vaten van het omliggende weefsel los te maken.

Hoewel de tandjes niet te scherp moeten zijn lijken me enigszins ribbelige tandjes niet vervelend omdat het weefsel dan iets beter gefixeerd wordt in de bek van het apparaat. Geen ervaring hier mee

Met vriendelijke groet,

Kind regards,

Roelf Postema  
Chirurg

Consultant surgeon

Telefoon 0181-658391  
E-mail rpostema@spijkennisemc.nlRuwaard van Puttenweg 500 | 3201 GZ Spijkennis  
Postbus 777 | 3200 GA Spijkennis  
website | nieuws | route

Figure 42: The email contact with surgeon Roelf Postema.

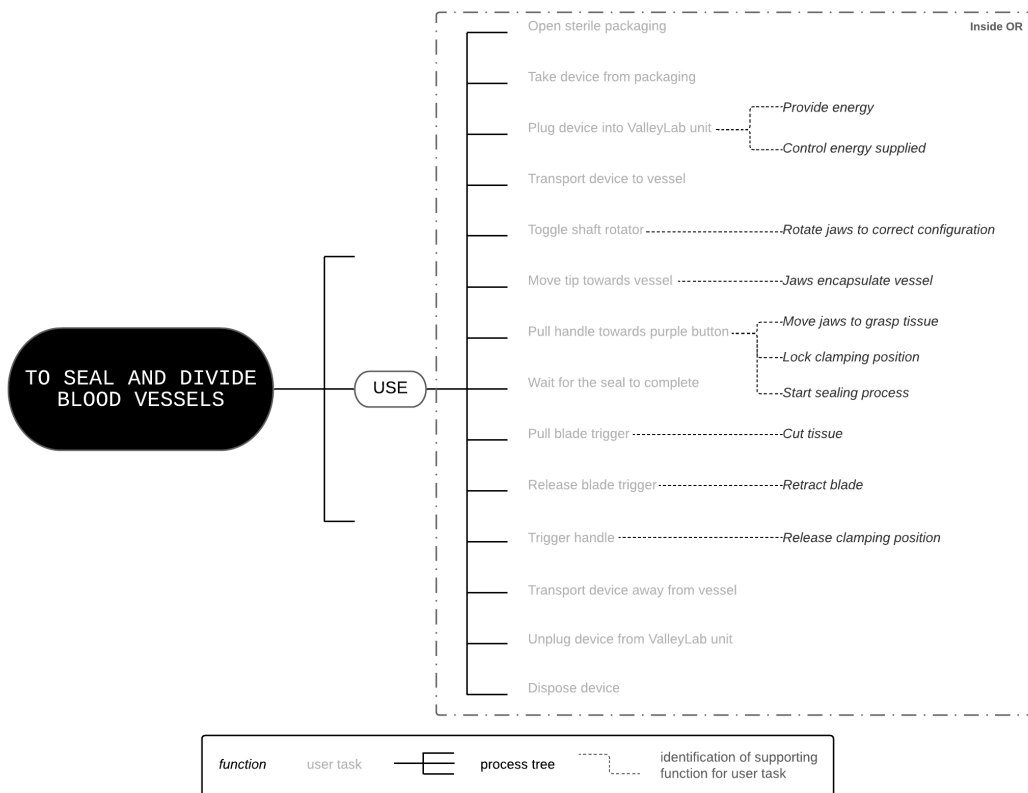


Figure 43: Step-by-step function analysis of the traditional bipolar vessel sealer. All the steps happen inside the operating theatre.

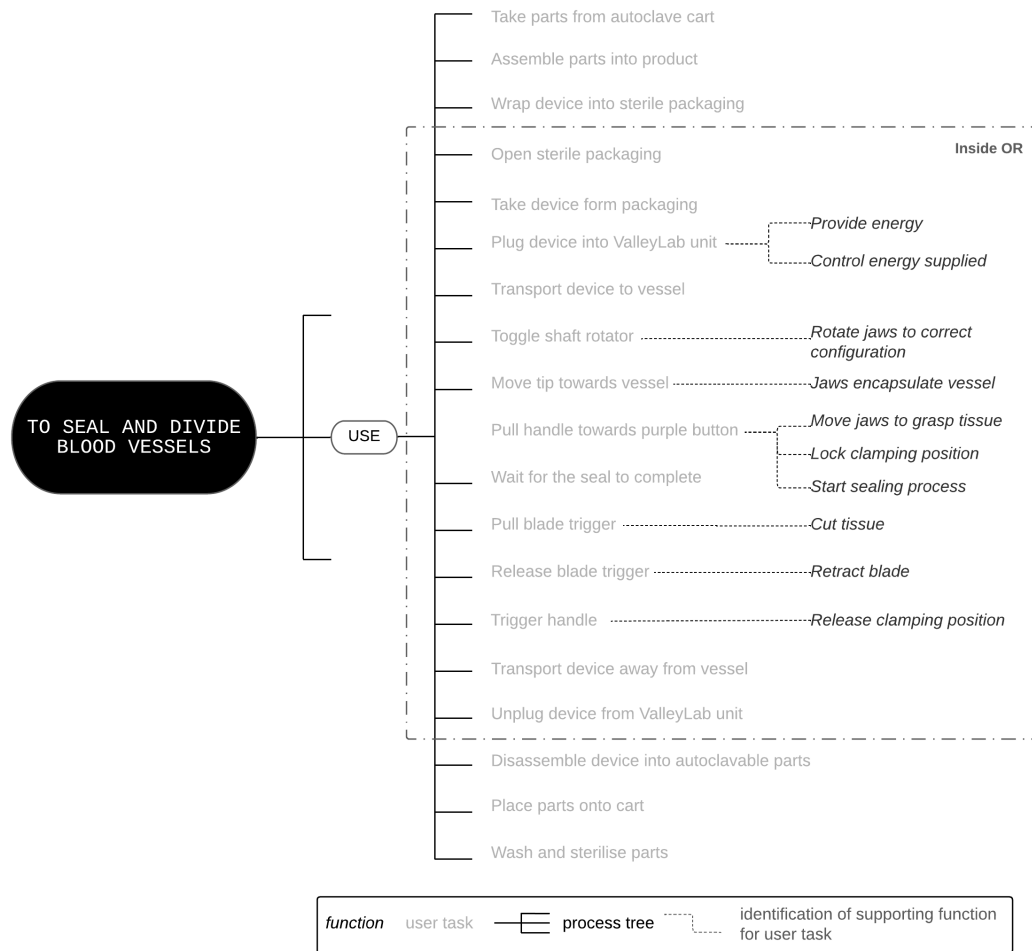


Figure 44: Step-by-step function analysis of the bipolar vessel sealer to be designed. A distinction is made between steps that happen inside the operating theatre and steps that happen outside the operating theatre.

<b>F<sub>n</sub></b>		<b>65.50</b>	<b>N</b>
<b>opening angle <math>\beta</math></b>		<b>0</b>	<b>degrees</b>
<b>a</b>	length jaw	<b>22.24</b>	<b>mm</b>
<b>h</b>	interpivot length	<b>2.01</b>	<b>mm</b>
<b>i</b>	57 - beta	<b>57</b>	
<b>R<sub>n</sub></b>	arm F <sub>n</sub>	<b>22.24</b>	<b>mm</b>
	$a \cdot \cos(\beta)$		
<b>R<sub>p</sub></b>	arm F <sub>push</sub>	<b>1.686</b>	<b>mm</b>
<b>F<sub>p</sub></b>		<b>864.1</b>	<b>N</b>
<b>slope angle <math>\theta</math></b>		<b>22.5</b>	<b>degrees</b>
<b>F<sub>pX</sub></b>	$F_p \cdot \sin(\theta)$	<b>330.7</b>	<b>N</b>
<b>F<sub>pY</sub></b>	$F_p \cdot \cos(\theta)$	<b>798.4</b>	<b>N</b>
<b>'mg' force</b>		<b>935.3</b>	<b>N</b>
<b>force slope down</b>		<b>357.9</b>	<b>N</b>
<b>F<sub>push</sub> along slope</b>		<b>357.9</b>	<b>N</b>
<b>F<sub>pushX</sub></b>		<b>330.7</b>	<b>N</b>

Table 5: The Excel file used to calculate  $F_{pushX}$  with the occlusion force model.

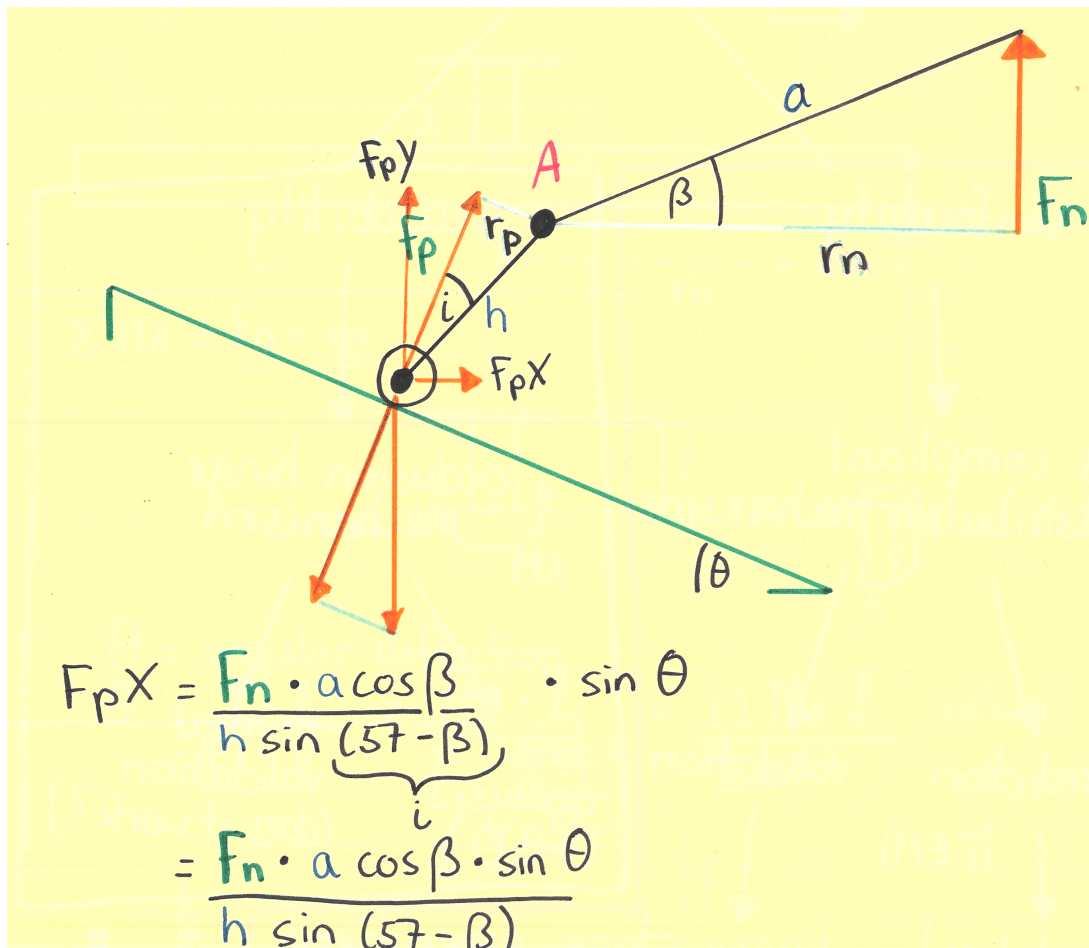


Figure 45: Free Body Diagram balancing the forces exerted by the occlusion mechanism.

**values**

AB=CD	23,8	mm
BD	82,05	mm
AC	121,75	mm
E	190000	N/mm <sup>2</sup>
b	15,5	mm
h	0,3	mm
l	0,034875	mm
L	4,85	mm

**input**

angle theta	20	degrees
-------------	----	---------

BE	8,140079	mm
BC	99,71811	mm

**area BCD**

S	102,7841	mm
A	718,3843	mm <sup>2</sup>
FD	14,4083	mm

**angles**

ABE	70	degrees
EBC	85,31768	degrees
CBD	10,1138	degrees
<b>B</b>	165,4315	degrees

BDF	79,8862	degrees
CDF	52,74303	degrees
<b>D</b>	132,6292	degrees

BCE	4,682316	degrees
DCF	37,25697	degrees
<b>C</b>	41,93929	degrees

**QUICK ANSWER ANGLES**

A	20	degrees
B	165,4315	degrees
C	41,93929	degrees
D	132,6292	degrees

**NEUTRAL ANGLES**

A=C	33,48465	degrees
B=D	146,5153	degrees

**CHANGE IN ANGLE**

A	-13,4847	degrees
B	18,91614	degrees
C	8,454631	degrees
D	-13,8861	degrees

**CHANGE IN MOMENT**

Ta	-643,092	Nm
Tb	902,1236	Nm
Tc	403,207	Nm
Td	-662,238	Nm

**FORCE APPLIED**

distance from B	10	mm
distance from D	10	mm
near B	90,21236	N
near D	-66,22384	N

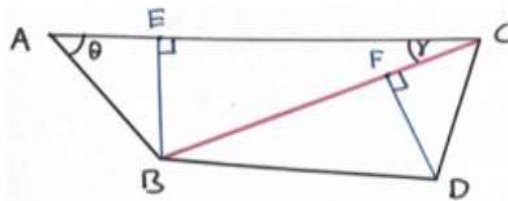
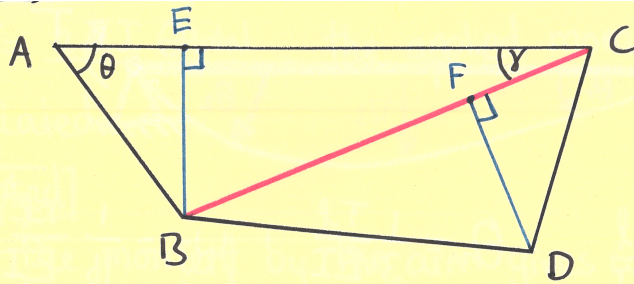


Figure 46: The Excel file containing the mathematical model of the angular translation in a trapezium. When angle  $\theta$  is entered as input it calculates the other three angles in the trapezium. Knowing the neutral angles of the trapezium in rest, the model calculates the angles of deflection and relates these to the amount of force applied to the mechanism using the material properties of the deflecting parts.



We know  $AB, BD, CD, AC$  ;

$$BE = AB \sin \theta$$

Using the Law of Cosines :

$$BC^2 = AB^2 + AC^2 - 2 \cdot AB \cdot AC \cdot \cos \theta$$

$$BC = \sqrt{AB^2 + AC^2 - 2 \cdot AB \cdot AC \cdot \cos \theta}$$

Now that we know  $BC$ , we can calculate the area of  $\triangle BCD$  using Heron's formula:

$$S (\text{semiperimeter}) = \frac{BC + BD + CD}{2}$$

$$A_{BCD} = \sqrt{s(s-BC)(s-BD)(s-CD)}$$

Now that we know the area of  $\triangle BCD$ , we can calculate  $FD$  using  $A = \frac{1}{2}bh$  ;

$\frac{1}{2}bh$  translates to  $A = \frac{1}{2} \cdot BC \cdot FD$ , so :

$$FD = \frac{2A}{BC}$$

Because we know all lengths of our irregular quadrilateral, we can calculate all angles using basic trigonometry.

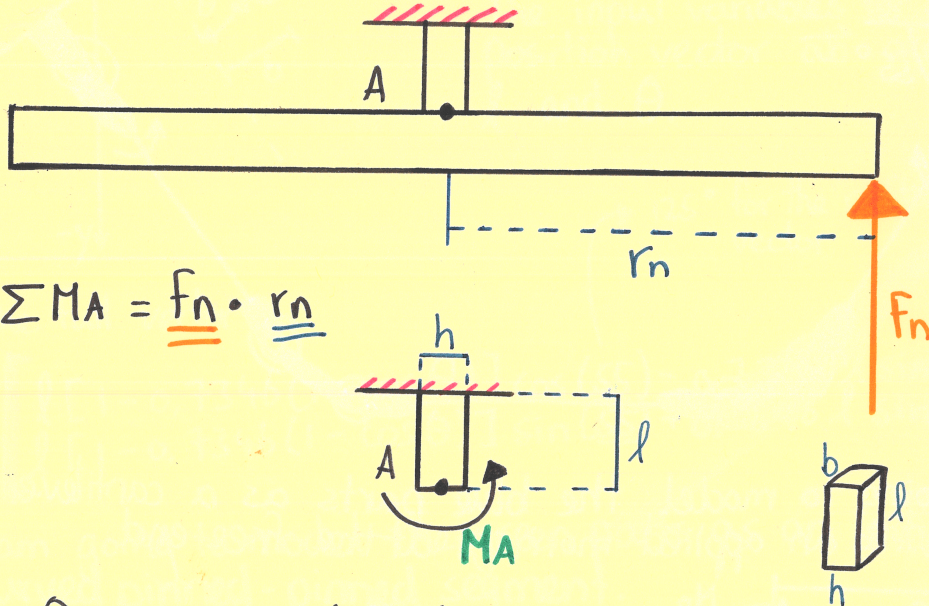
Next, we have to link the change in angle to the moment applied.

Figure 47: The theory behind the angle translation model. It uses the Law of Cosines, Heron's formula and the relation between the base and the height of a triangle to calculate the length of the inner arms  $BC$ ,  $BE$  and  $DF$ , knowing the length of the four outer arms. From this, all internal angles can be calculated using Pythagoras' theorem.

# prediction of compliant distribution mechanisms

↳ analytical models

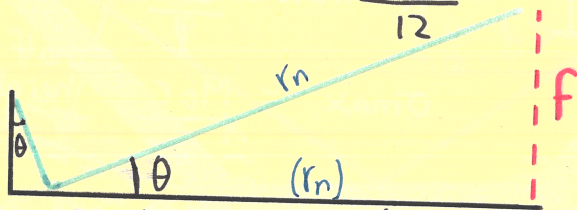
spring toy



$$\Sigma MA = \underline{F_n} \cdot \underline{r_n}$$

$\theta$  = angular deflection

$$\theta = \frac{T \cdot l}{E \cdot I} = \frac{MA \cdot l}{E \cdot \frac{b \cdot h^3}{12}} = \frac{12 MA l}{E b h^3} \text{ radians}$$



$f$  = deflection of the tip

$$f = r_n \sin(\theta) \text{ radians}$$

$$f = r_n \sin\left(\frac{12 MA l}{E b h^3}\right) = r_n \sin\left(\frac{12 F_n r_n l}{E b h^3}\right) \text{ radi}$$

$$f = r_n \sin\left(\frac{12 MA l}{E b h^3} \cdot \left[\frac{180}{\pi}\right]\right) = \left[ r_n \sin\left(\frac{2160 MA l}{E b h^3 \pi}\right) \right] \text{ degrees}$$

Figure 48: Analytical model for the deflection of the spring toy. The horizontal beam is assumed completely rigid. The vertical beam deflects when a force  $F_n$  is exerted.

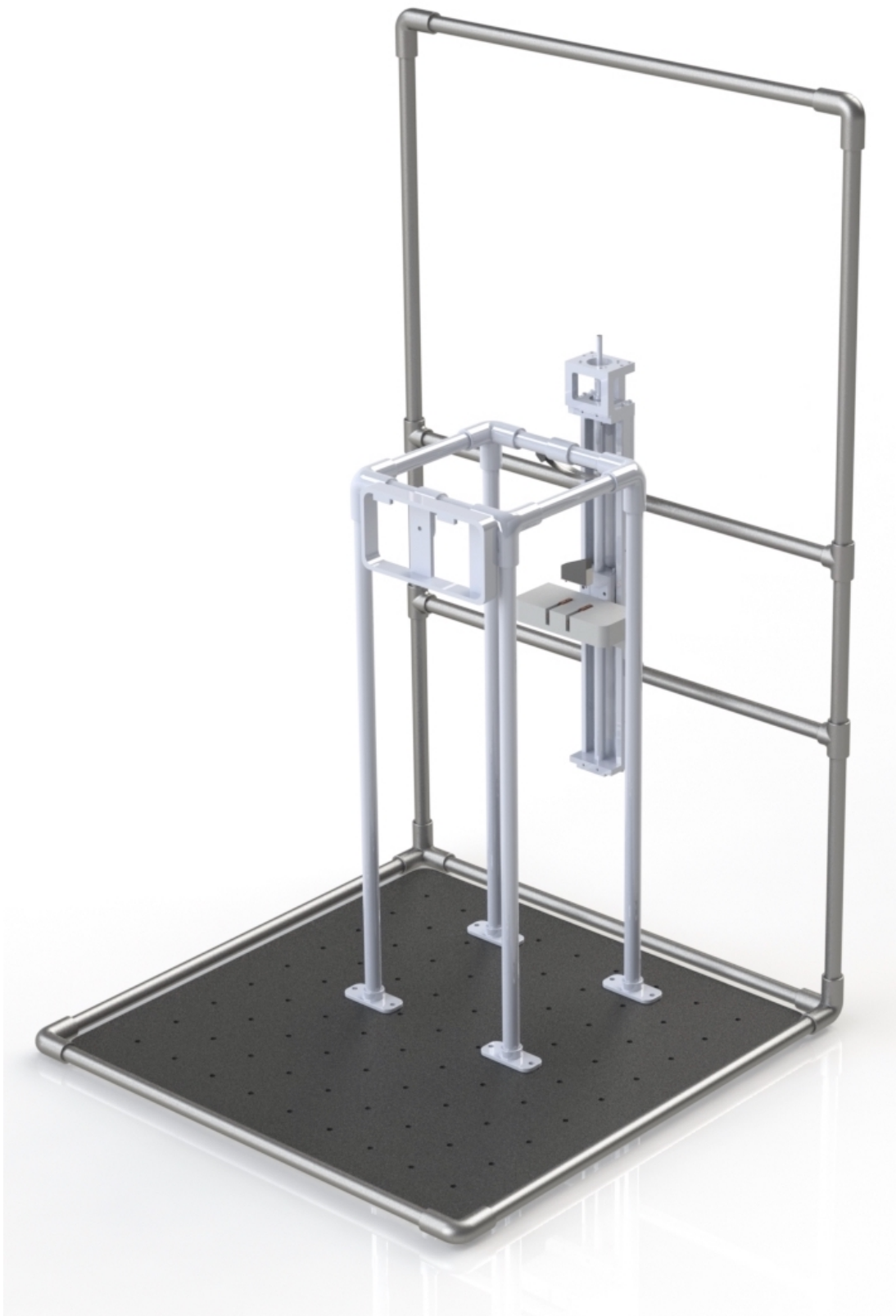


Figure 49: Overview rendering of the experiment setup.



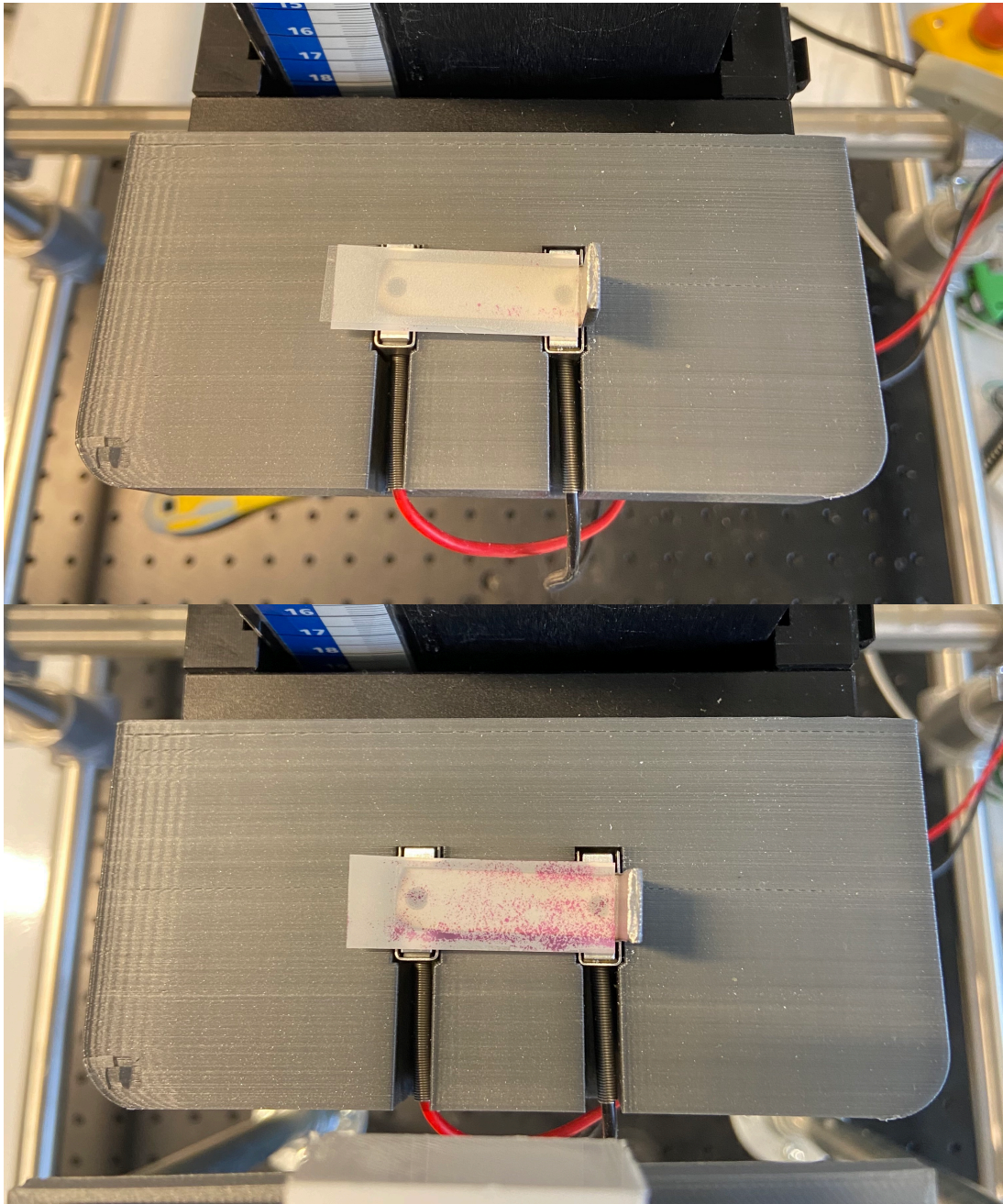


Figure 50: The FujiFilm 5LW pressure-sensitive film before (top) and after (bottom) pressure has been applied for 5 seconds. Note how the purple dots have developed on the pressure hotspots around the edges and the setting screws.

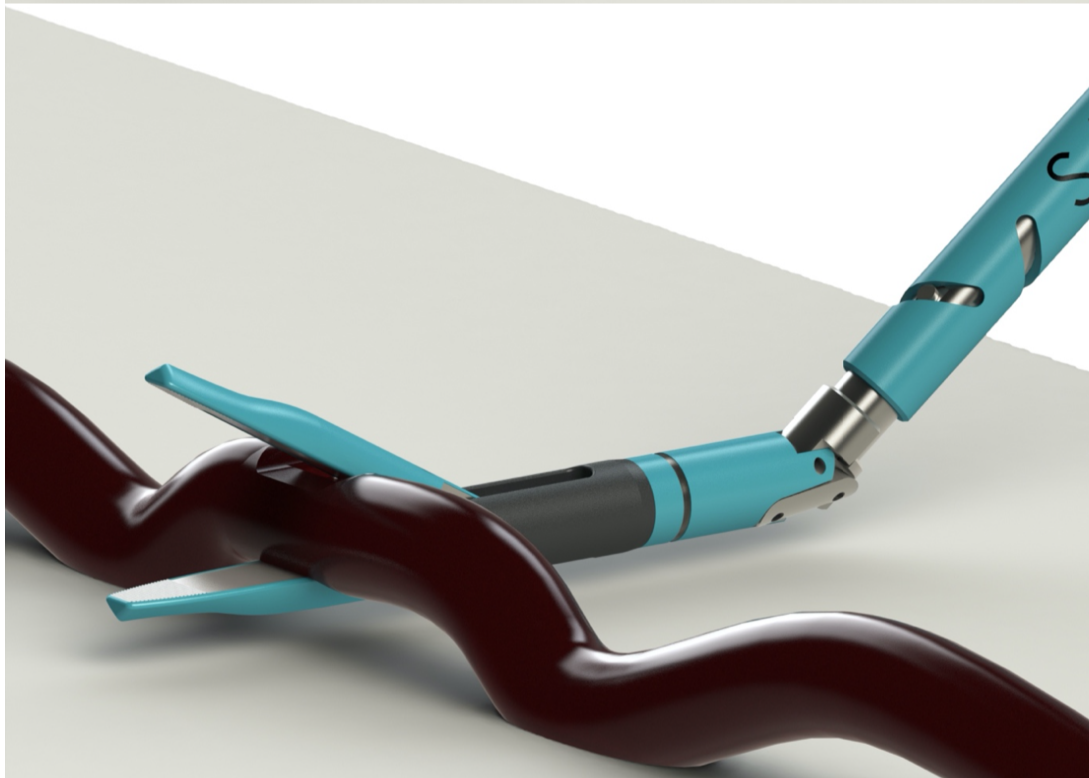
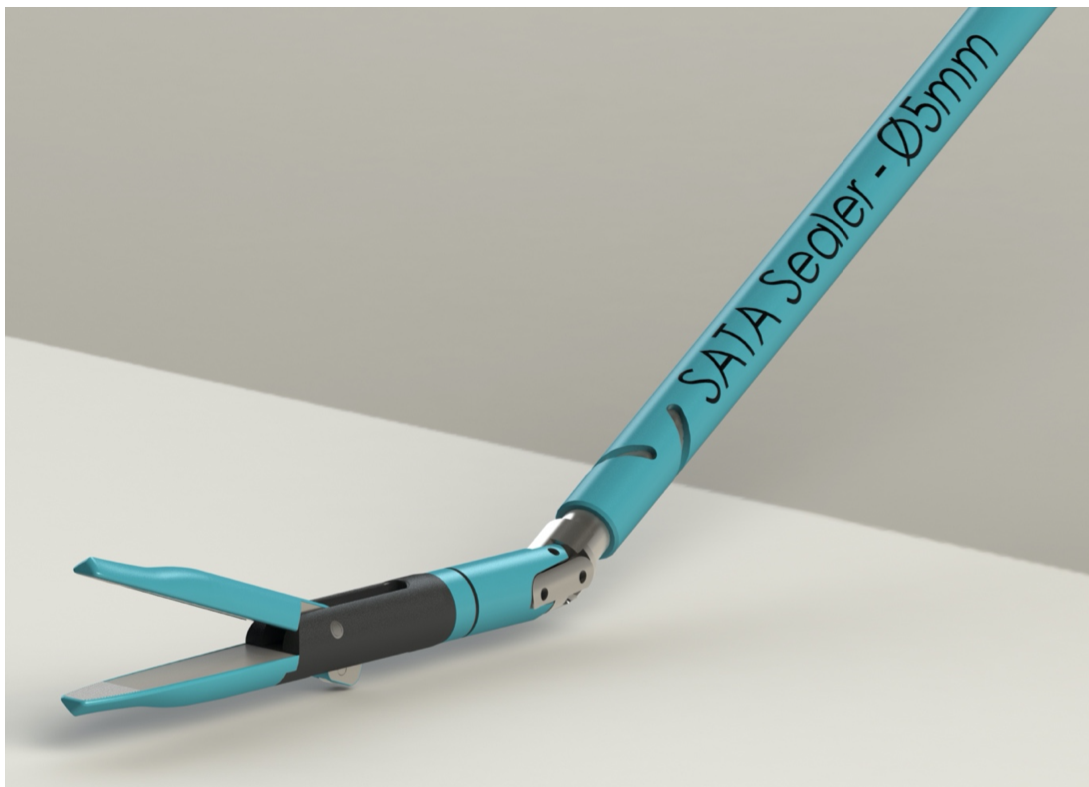


Figure 51: The steerable and reusable bipolar vessel sealer by Philip de Haes [26].

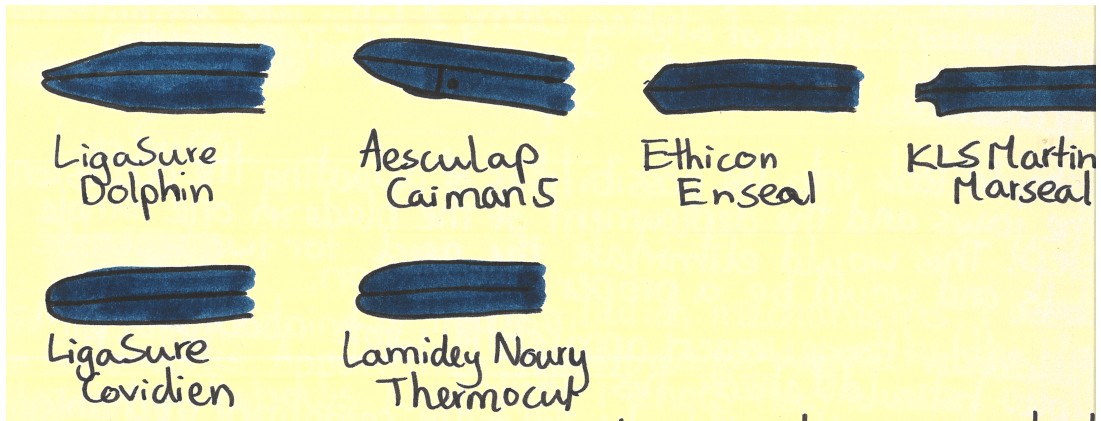


Figure 52: A variety of shapes of BVS jaws on the market seen from the sagittal (side) plane.

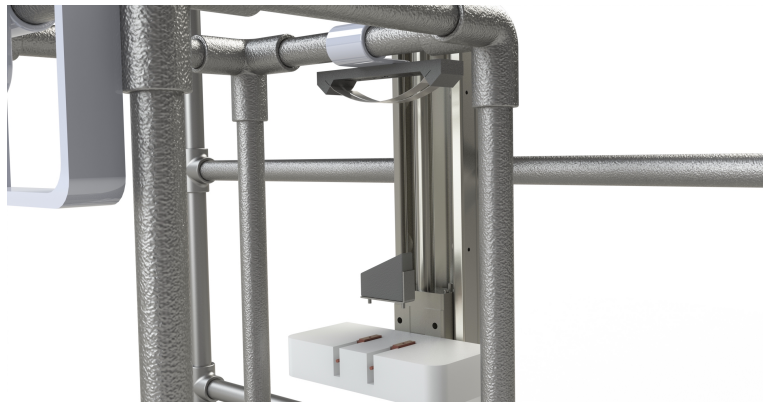


Figure 53: A rendering of the experiment setup showing the phantom support with the load cells inserted. The steel plate with the silicon phantom tissue floats above the phantom support. At the top of the image, the leaf spring mechanism can be seen attached to the support rig.

## B Pressure distribution experiment - lab report

### B.1 Introduction

This experiment was conducted to test which of the three compliant mechanisms distributes pressure most effectively when clamping a piece of phantom tissue. The incentive behind this experiment is that conventional bipolar vessel sealing devices distribute pressure poorly, negatively affecting the quality of the seal (=burst pressure) [2][1]. The objective of this experiment is to determine which mechanism should be incorporated into the redesign of the bipolar vessel sealer. The research question is:

”Which of the three compliant mechanisms performs best at distributing pressure uniformly in a clamping configuration?”

### B.2 Materials

The following equipment was used to perform the experiment:

- Support rig (scaffolding tubes and connective pieces)
- Bottom plate
- Linear stage (Aerotech PRO115-400-UF)
- Compliant mechanisms (spring toy/trapezium/leaf spring)
- Silicon phantom tissue (Ecoflex 00-50)
- Phantom support with space for load cells
- Steel plate connected to load cells
- Pressure sensitive film (FujiFilm Prescale 5LW)
- 2 load cells (FUTEK S-Beam) with the accompanying electronics
- Laptop with LabVIEW 2018
- Thermometer
- Hygrometer

### B.3 Method

1. Prepare silicon phantom tissue according to the instructions.
2. Assemble the setup according to figure 49. The moving part of the linear stage is attached to the phantom support plate that carries the phantom tissue. The compliant mechanism is attached to the top part of the rig that is secured to the bottom plate.
3. Set up the load cells and insert them into the phantom support. Fix them using bolts.
4. Make sure the FujiFilm Prescale has been in the correct environment for at least 30 minutes. Assemble the FujiFilm Prescale according to the instructions and place on the surface of the steel plate.
5. Place the phantom tissue onto the steel place.
6. Measure the temperature ( $^{\circ}\text{C}$ ) and the relative humidity (RH%) of the room.

7. Program the linear stage to approach the mechanism with the optimal force of 7 N. The time from first contact to final position should be 5 seconds (the pressure should increase gradually to the required level in 5 seconds). This required level of pressure should be maintained for another 5 seconds. After 5 seconds, the linear stage can be retracted.
8. Remove the FujiFilm Prescale and disassemble according to the instructions.
9. Save the data obtained by the load cells.
10. Repeat step 4-7 for five times with all three distribution mechanisms and all three phantoms.

#### **B.4 Control treatment**

An inclined rigid beam is used to check whether the newly designed mechanisms outperform the conventional clamping situation.

#### **B.5 Calibration of load cells**

To measure the forces under either side of the phantom, two Futek Miniature S-Beam Jr. Load Cells were used, both capable of sensing force up to 9 N. To use these sensors, a circuit had to be built, containing a NI USB-6008 Multifunction I/O device and two Scaime CPJ strain gauge conditioners. These devices contain a 10 Hz low-pass filter to attenuate the signal and to reduce noise. After setting up the circuit with the required electronics, the load cells had to be calibrated. This was done using LabVIEW 2018 (the software used for data collection), Microsoft Excel and a set of weights. A list was created containing the mass of the different weights, the corresponding force values and the voltages measured when these weights were placed on top of the load cells (each load cell individually). By creating a scatter plot, Excel revealed the two linear equations that fit the data points. The gradients of these equations were the calibration values that could be entered into LabVIEW to show corresponding force values when voltages were sensed.

The load cells always measure a certain value, also when no force is being exerted. This value depends on the load cell itself as well as certain objects that are mounted on top of them. In the case of this pressure distribution experiment, the steel plate and the film also exert downward pressure that has to be corrected for. This correction can be carried out by determination of an offset value and entering this value into LabVIEW.

## C Results tables

	1	2	3	4	5	AVG
<b>CP</b>	0.885	0.899	0.9	0.904	0.899	<b>0.90</b>
<b>LSP</b>	0.477	0.478	0.519	0.519	0.528	<b>0.50</b>
<b>STP</b>	2.251	2.233	2.261	2.265	2.251	<b>2.25</b>
<b>TP</b>	0.347	0.347	0.357	0.357	0.361	<b>0.35</b>
<b>CF</b>	0.408	0.422	0.418	0.404	0.358	<b>0.40</b>
<b>LSF</b>	0.293	0.32	0.312	0.307	0.307	<b>0.31</b>
<b>STF</b>	0.21	0.2	0.2	0.196	0.205	<b>0.20</b>
<b>TF</b>	6.938	6.934	6.98	6.912	6.866	<b>6.93</b>
<b>CR</b>	2.394	2.651	3.829	2.83	2.565	<b>2.85</b>
<b>LSR</b>	0.981	0.881	0.88	0.931	0.963	<b>0.93</b>
<b>STR</b>	1.265	1.274	1.311	1.269	1.306	<b>1.29</b>
<b>TR</b>	1.756	1.654	1.645	1.572	1.522	<b>1.63</b>

Table 6: Table containing the measured differences in force (N) between the load cells for every mechanism/phantom combination. The last column shows the average values of the five measurements.

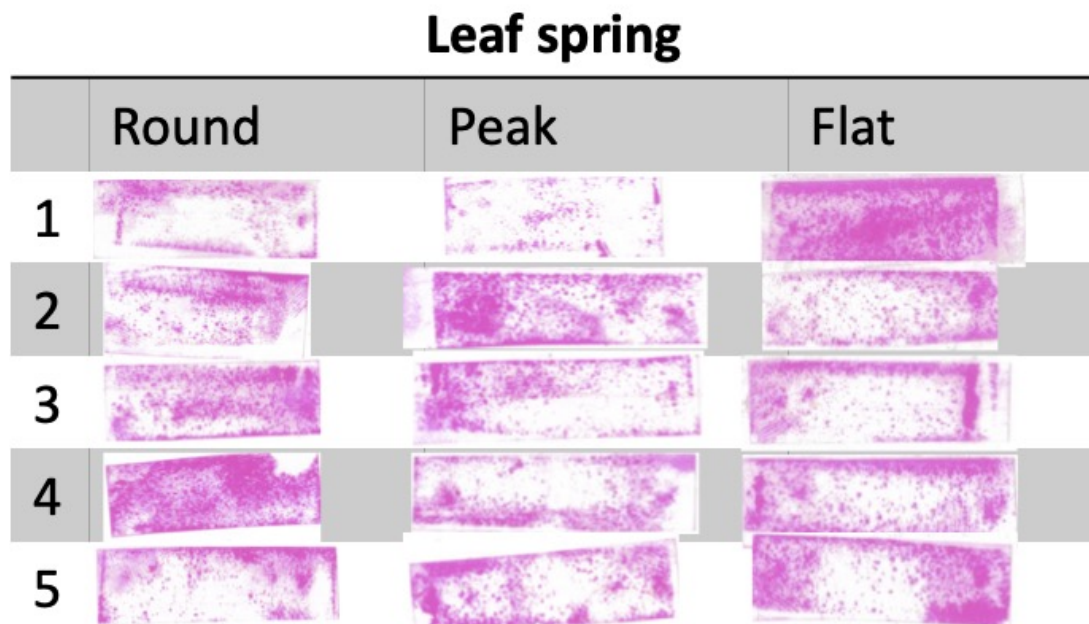
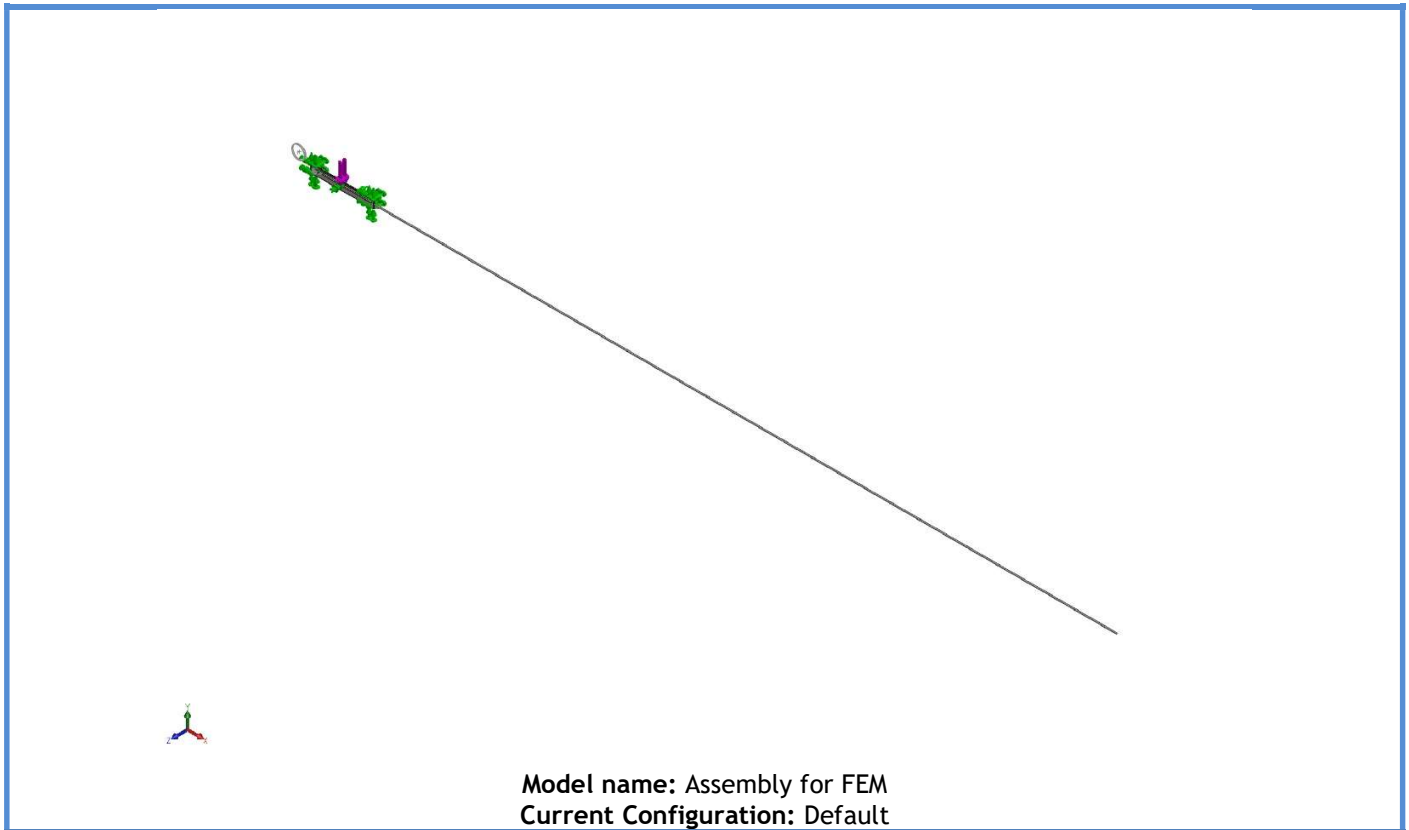
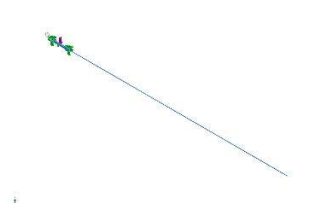
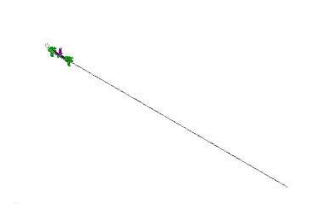


Figure 54: The pressure-sensitive film results of the leaf spring mechanism.



**Solid Bodies**

Document Name and Reference	Treated As	Volumetric Properties	Document Path/Date Modified
Fillet8 	Solid Body	Mass:0 000764747 kg Volume:9 7367e-08 m <sup>3</sup> Density:7,854 27 kg/m <sup>3</sup> Weight:0 00749452 N	C:\Users\Jim Cross\Documents\Gradd\B lade - steep slope but short.SLDPRT Jan 10 09:40:07 2022
Boss-Extrude1 	Solid Body	Mass:1 25664e-05 kg Volume:1 5708e-09 m <sup>3</sup> Density:8,000 kg/m <sup>3</sup> Weight:0 00012315 N	C:\Users\Jim Cross\Documents\Gradd\O cclusion hinge test print\Occlusion hinge print axis.SLDPRT Oct 28 09:46:00 2021



## Study Properties

Study name	Static 1
Analysis type	Static
Mesh type	Solid Mesh
Thermal Effect:	On
Thermal option	Include temperature loads
Zero strain temperature	298 Kelvin
Include fluid pressure effects from SOLIDWORKS Flow Simulation	Off
Solver type	FFEPlus
Inplane Effect:	Off
Soft Spring:	Off
Inertial Relief:	Off
Incompatible bonding options	Automatic
Large displacement	Off
Compute free body forces	On
Friction	Off
Use Adaptive Method:	Off
Result folder	SOLIDWORKS document (C:\Users\Jim Cross\Documents\Gradd)

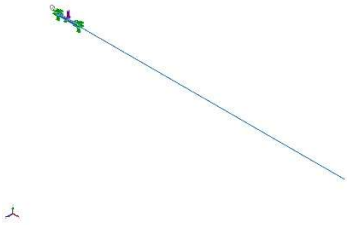
## Units

Unit system:	SI (MKS)
Length/Displacement	mm
Temperature	Kelvin
Angular velocity	Rad/sec
Pressure/Stress	N/m <sup>2</sup>






### Material Properties

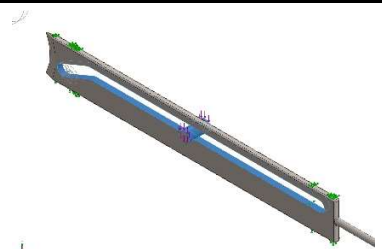
Model Reference	Properties	Components
	<p><b>Name:</b> AISI 316 Stainless Steel Sheet (SS)  <b>Model type:</b> Linear Elastic Isotropic  <b>Default failure criterion:</b> Unknown  <b>Yield strength:</b> 1 72369e+08 N/m<sup>2</sup>  <b>Tensile strength:</b> 5 8e+08 N/m<sup>2</sup>  <b>Elastic modulus:</b> 1 93e+11 N/m<sup>2</sup>  <b>Poisson's ratio:</b> 0 27  <b>Mass density:</b> 8,000 kg/m<sup>3</sup>  <b>Thermal expansion coefficient:</b> 1 6e-05 /Kelvin</p>	<p>SolidBody 1(Fillet8)(Blade - steep slope but short-1), SolidBody 1(Boss-Extrude1)(Occlusion hinge print axis-1)</p>
Curve Data:N/A		

### Loads and Fixtures

Fixture name	Fixture Image	Fixture Details
Fixed-1		<b>Entities:</b> 2 face(s) <b>Type:</b> Fixed Geometry

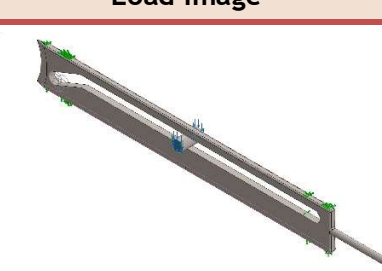
#### Resultant Forces

Components	X	Y	Z	Resultant
Reaction force(N)	-6 5653e-06	798 4	-7 72016	798 437
Reaction Moment(N.m)	0	0	0	0

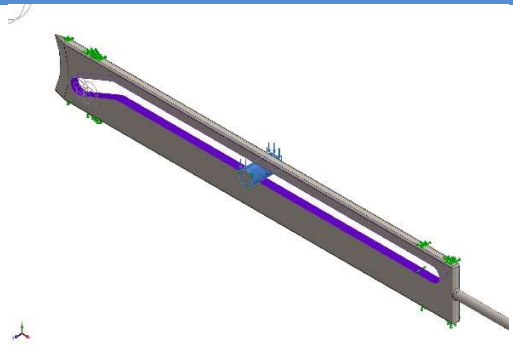
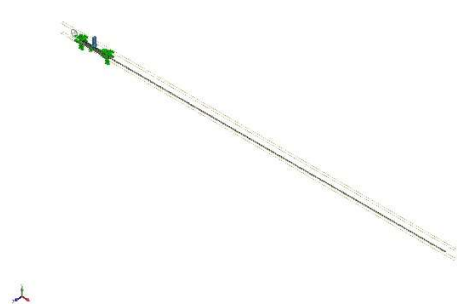
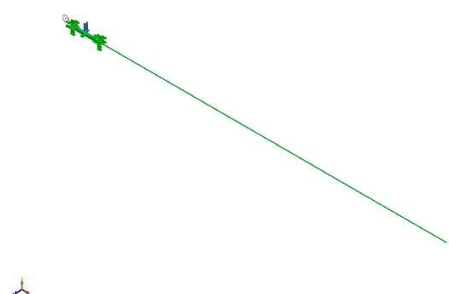
Roller/Slider-2		<b>Entities:</b> 2 face(s) <b>Type:</b> Roller/Slider
-----------------	--	--

#### Resultant Forces

Components	X	Y	Z	Resultant
Reaction force(N)	0 000604599	-0 000151707	7 72008	7 72008
Reaction Moment(N.m)	0	0	0	0

Load name	Load Image	Load Details
Force-1		<b>Entities:</b> 2 face(s) <b>Reference:</b> Face< 1 > <b>Type:</b> Apply force <b>Values:</b> ---; ---; -,798 4 N

Contact Information

Contact	Contact Image	Contact Properties		
Contact Set-1		<p><b>Type:</b> No Penetration contact pair</p> <p><b>Entities:</b> 2 face(s)</p> <p><b>Advanced:</b> Node to surface</p>		
<b>Contact/Friction force</b>				
<b>Components</b>	<b>X</b>	<b>Y</b>	<b>Z</b>	<b>Resultant</b>
Contact Force(N)	-1 4672E-14	6 1108E-13	-1 7699E-25	6 1126E-13
Global Contact		<p><b>Type:</b> Bonded</p> <p><b>Components:</b> 1 component(s)</p> <p><b>Options:</b> Incompatible mesh</p>		
Component Contact-1		<p><b>Type:</b> No penetration (Surface to surface)</p> <p><b>Components:</b> 2 Solid Body (s)</p>		

## Mesh information

Mesh type	Solid Mesh
Mesher Used:	Standard mesh
Automatic Transition:	Off
Include Mesh Auto Loops:	Off
Jacobian points for High quality mesh	16 Points
Element Size	0.530655 mm
Tolerance	0.0265327 mm
Mesh Quality	High
Remesh failed parts with incompatible mesh	Off

## Mesh information - Details

Total Nodes	25022
Total Elements	10753
Maximum Aspect Ratio	17.674
% of elements with Aspect Ratio < 3	90.3
Percentage of elements with Aspect Ratio > 10	0.102
Percentage of distorted elements	0
Time to complete mesh(hh:mm:ss):	00:00:05
Computer name:	

## Resultant Forces

### Reaction forces

Selection set	Units	Sum X	Sum Y	Sum Z	Resultant
Entire Model	N	0.000598034	798.4	-9.25064e-05	798.4

### Reaction Moments

Selection set	Units	Sum X	Sum Y	Sum Z	Resultant
Entire Model	N.m	0	0	0	0

### Free body forces

Selection set	Units	Sum X	Sum Y	Sum Z	Resultant
Entire Model	N	0.000622834	9.53674e-07	-7.72476e-05	0.000627606

### Free body moments

Selection set	Units	Sum X	Sum Y	Sum Z	Resultant
Entire Model	N.m	0	0	0	1e-33

## Beams

No Data



### Study Results

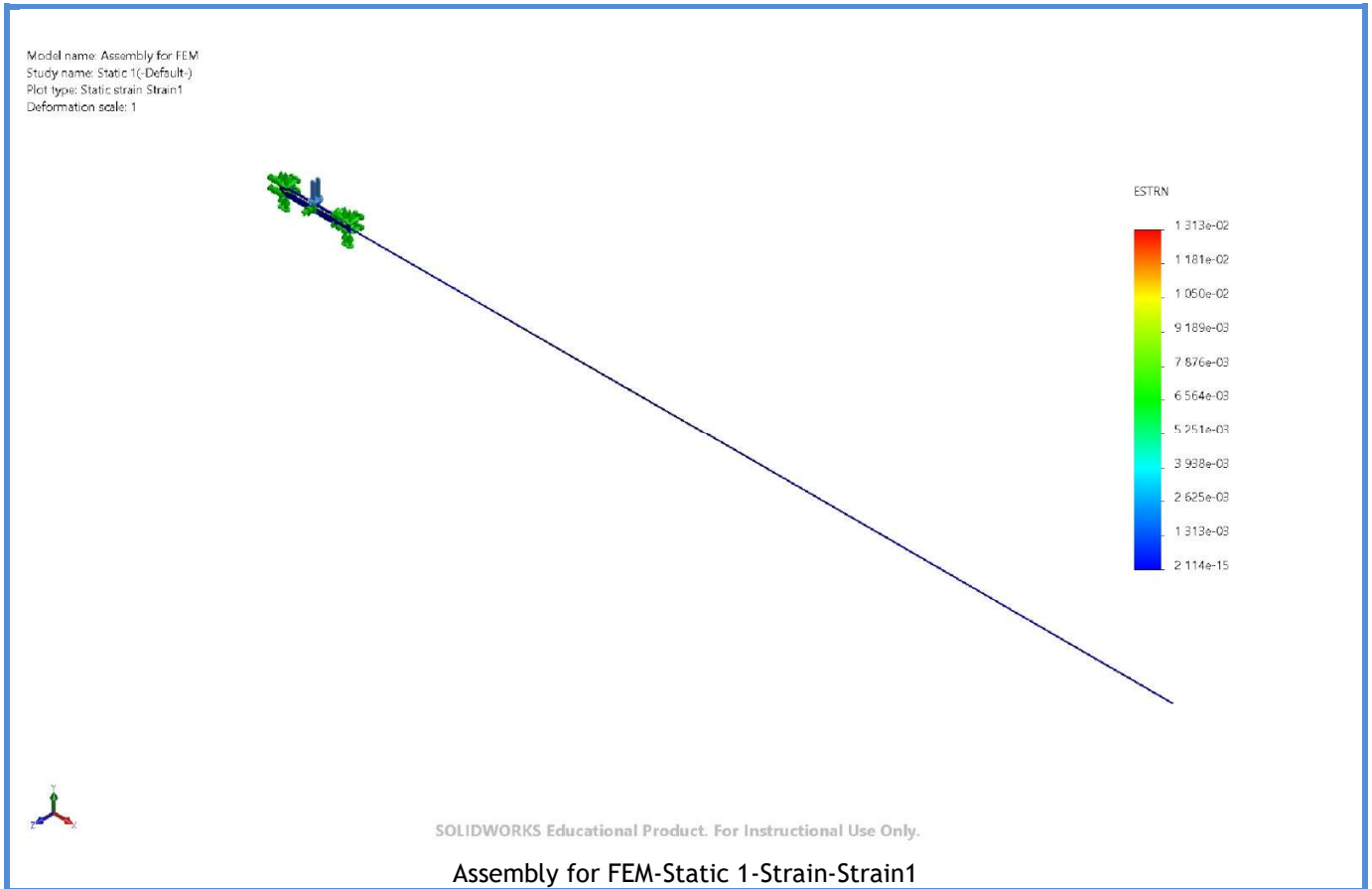
Name	Type	Min	Max
Stress1	VON: von Mises Stress	5 191e-04N/m <sup>2</sup> Node: 21702	2 675e+09N/m <sup>2</sup> Node: 10427



Name	Type	Min	Max
Displacement1	URES: Resultant Displacement	0 000e+00mm Node: 3716	5 901e-02mm Node: 24844



Name	Type	Min	Max
Strain1	ESTRN: Equivalent Strain	2.114e-15 Element: 3489	1.313e-02 Element: 105



Name	Type
Displacement1{1}	Deformed shape



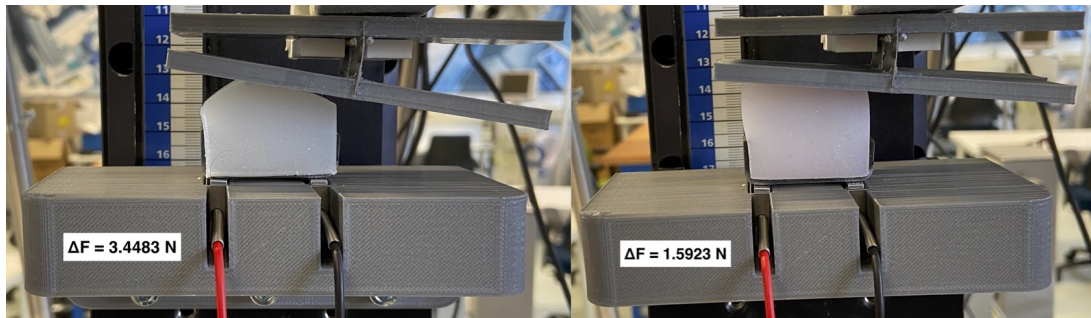


Figure 55: Results when the flat and peak phantom are not placed in the middle on the mechanism. The spring toy/peak combination gives a  $\Delta F$  of 3.45 N and the spring toy/flat combination shows a difference of 1.59 N. In both cases, the left load cells measured more force than the right load cell.

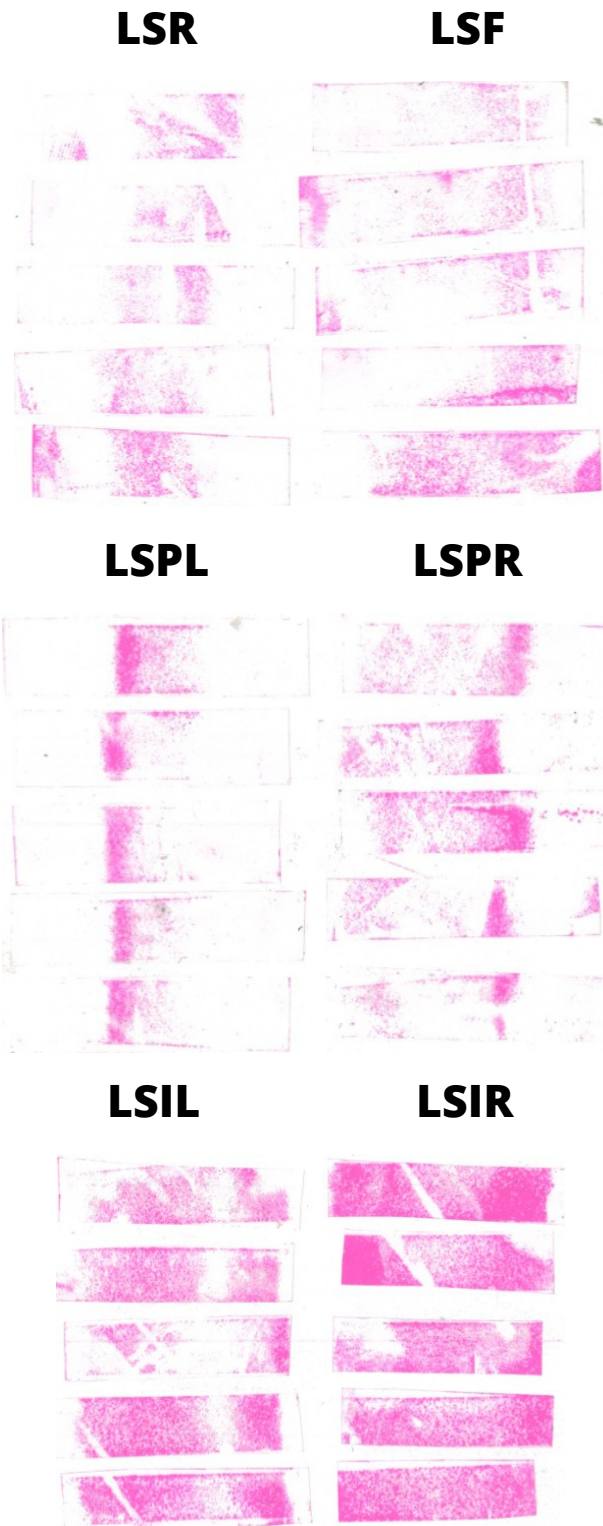


Figure 56: Pressure sensitive film measurements with the leaf spring mechanism taken from the top surface for the phantoms. Starting top left: round, flat, peak (left), peak (right), incline (left), incline (right).

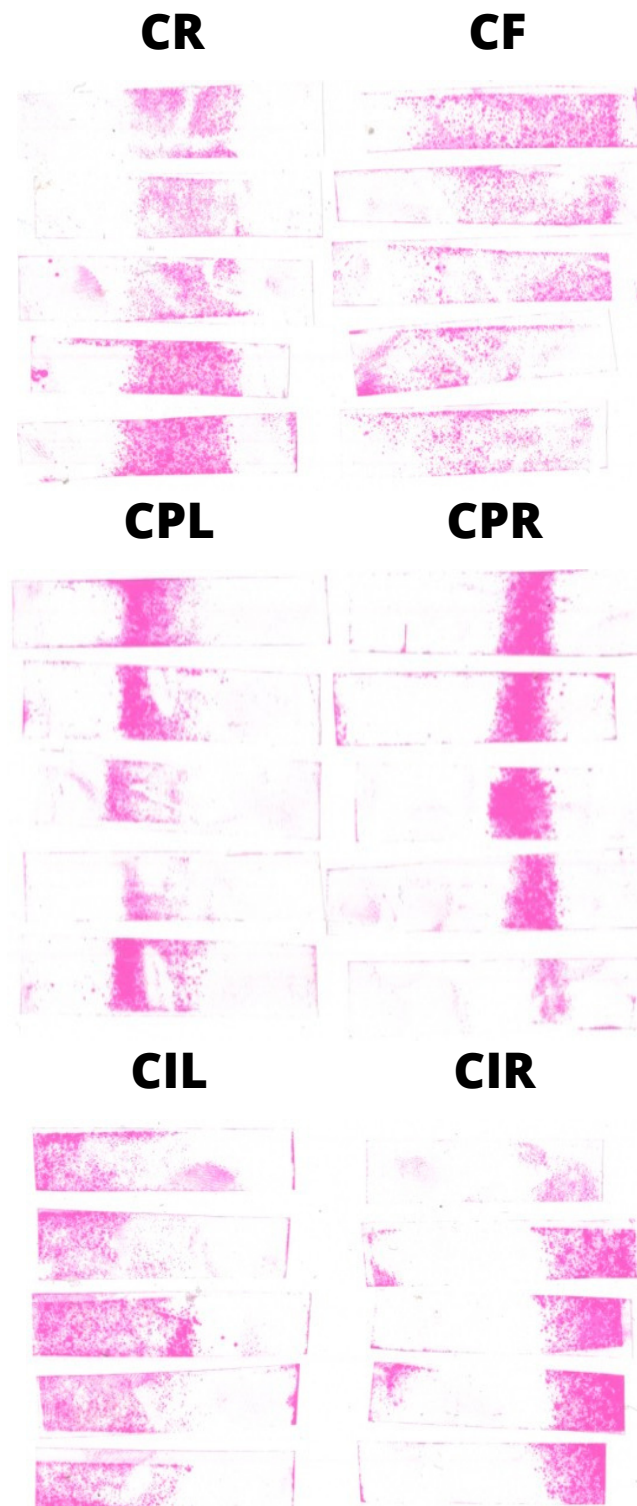


Figure 57: Pressure sensitive film measurements with the control mechanism taken from the top surface for the phantoms. Starting top left: round, flat, peak (left), peak (right), incline (left), incline (right).